

Incorporating Lindblad Decay Dynamics into Mixed Quantum-Classical Simulations

Eric R. Koessler,^{1, a)} Arkajit Mandal,^{1, 2} and Pengfei Huo^{1, 3, b)}

¹⁾*Department of Chemistry, University of Rochester, 120 Trustee Road, Rochester, NY 14627*

²⁾*Department of Chemistry, Columbia University, New York, NY 10027, U.S.A.*

³⁾*The Institute of Optics, Hajim School of Engineering, University of Rochester, Rochester, New York, 14627*

We derive the \mathcal{L} -MFE method to incorporate Lindblad jump operator dynamics into the mean-field Ehrenfest (MFE) approach. We map the density matrix evolution of Lindblad dynamics onto pure state coefficients using trajectory averages. We use simple assumptions to construct the \mathcal{L} -MFE method that satisfies this exact mapping. This establishes a method that exactly reproduces Lindblad decay dynamics using a wavefunction description, with deterministic changes of the magnitudes of the quantum expansion coefficients, while only adding on a stochastic phase. We further demonstrate that when including nuclei in the Ehrenfest dynamics, the \mathcal{L} -MFE method gives semi-quantitatively accurate results, with the accuracy limited by the accuracy of the approximations present in the semiclassical MFE approach. This work provides a general framework to incorporate Lindblad dynamics into semiclassical or mixed quantum-classical simulations.

I. INTRODUCTION

Accurately and efficiently simulating the quantum dynamics of an open quantum system remains a challenging task in modern quantum physics and chemical physics, due to the unfavorable exponential scaling of the quantum problem. To resolve this challenge, mixed quantum-classical (MQC) approaches^{1,2} have been developed by treating the crucial part of the system as the quantum subsystem, and the other parts as classical degrees of freedom (DOFs). This type of approach is particularly successful for describing non-adiabatic molecular dynamics that involve electronic-nuclear interactions, given the fact that the nuclear DOFs are in general anharmonic and their interactions with the electronic DOFs are non-Markovian, thus rendering many approximate master equations not directly applicable. One major category of these mixed quantum-classical methods is surface hopping, most notably Tully's fewest-switches surface hopping approach³ and several later additions to this method.^{1,4,5} Another major category is the mean-field Ehrenfest (MFE) approach,⁶ or more generally, semiclassical mapping approaches based on the Meyer-Miller mapping formalism.⁷⁻⁹ All of these approaches explicitly propagate the classical DOFs and captures their influence on the quantum DOFs through the parametric dependence of the quantum equations of motion (EOM) on the classical trajectories.

At the same time, the quantum subsystem, in principle, can also interact with other environmental DOFs. Example of these interacting environmental DOFs include the interaction of the electromagnetic field with molecules that causes spontaneous emission¹⁰⁻¹² and far-field electromagnetic modes that couple to a quantized radiation mode inside an optical cavity that causes pho-

ton leakage.¹³⁻¹⁷ It is often desirable to implicitly capture the environmental influence on the dynamics and avoid simulating these environmental DOFs explicitly. Another example is the presence of high frequency vibrations in molecules¹⁸⁻²⁰ that are essentially Markovian for the subsystem dynamics. These high frequency vibrations, however, cause difficulties for MQC simulations due to the inadequate description of them using classical trajectories.^{18,19} A number of approaches seek to phenomenologically incorporate these effects of population decay from a higher energy state to a lower energy state through an imaginary Hamiltonian approach,^{15,21-26} incorporating *ad-hoc* first-order decay processes,²⁷⁻²⁹ or *a posteriori* probabilistic collapse into the ground state.³⁰ These approaches do not capture the full nature of the decay dynamics as they generally do not describe the dynamics of the ground state at the wavefunction level, or do not account for proper decoherence processes during the population decay dynamics.

When a Markovian approximation of the system-environment interaction is valid, the Lindblad master equation^{31,32} offers the most general and quantum mechanically valid description of an open system's quantum dynamics, as it guarantees the positivity and preserves the trace of the reduced density matrix.^{31,32} Thus, it is ideal to use this computationally efficient and analytically simple Lindblad master equation to describe the influence of those Markovian environmental DOFs on the quantum subsystem, while simultaneously using the MQC approximation to incorporate the influence of the anharmonic, non-Markovian nuclear DOFs on the quantum subsystem. Indeed, the density matrix hybrid method,¹⁸⁻²⁰ which is based on this idea, has been developed recently to study non-adiabatic dynamics by combining MQC methods and master equation approaches. Still, solving the Lindblad master equation with many states in the quantum system is computationally challenging, due to the need to propagate the density matrix in the Liouville space.

To reduce this unfavorable scaling related to density

^{a)}Electronic mail: ekoessle@ur.rochester.edu

^{b)}Electronic mail: pengfei.huo@rochester.edu

matrix propagation in the Liouville space, one can equivalently describe dynamics as a stochastic wavefunction in the open system's Hilbert space that exactly reproduces the reduced density matrix of the open system, thus reducing the cost of solving the same dynamics by utilizing an ensemble of trajectories in the Hilbert space. This is referred to as the unravelling of the master equation.^{33,34} It is well known that the Lindblad master equation can be equivalently expressed as the stochastic Schrödinger equation (SSE)^{35–37} with jump processes that captures the projective action of the environment on the system, which randomly collapses the system wavefunction into a pure system state. Through the trajectory average of a large number of realizations of the jump trajectories, the SSE generates identical reduced density matrix dynamics as the Lindblad master equation. However, due to the large fluctuations in population of the system, the SSE encounters numerical instability when combined with mixed quantum-classical approaches.³⁸ The Ehrenfest+R method^{10,11} was recently developed to simulate the electronic quantum subsystem coupled to the classical electromagnetic field in order to accurately describe spontaneous emission processes. It effectively captures Lindblad dynamics with a deterministic change of the magnitude of the quantum coefficients, and stochastic changes of the phases. The Ehrenfest+R method,¹⁰ however, cannot exactly reproduce the Lindblad master equation due to a specific choice of the off-diagonal decay rate.

In this paper, we develop a general framework for simulating Lindblad-type dynamics with a wavefunction description. As opposed to the SSE approaches that stochastically change both the magnitudes and the phases of the quantum expansion coefficients, our new method only stochastically changes the phases of the expansion coefficients, and exactly reproduces the jump operator dynamics of the Lindblad master equation. In particular, we give the derivation of a method to propagate the coefficients of the MFE method that fully agrees with Lindblad dynamics. The coefficient-propagation method derived using this framework is inspired by the Ehrenfest+R method;^{10–12,39,40} however, our approach exactly recovers Lindblad dynamics whereas the Ehrenfest+R approach does not. Additionally, we derive a simple fix to the approximations present in the Ehrenfest+R method and give rigorous justifications for particular algorithmic choices. Our wavefunction description of Lindblad dynamics can be seamlessly integrated into mixed quantum-classical methods that simulate coupled electronic-nuclear dynamics, such as the mean-field Ehrenfest approach, and we refer to this particular approach as the \mathcal{L} -MFE method. We have tested the accuracy, efficiency, and robustness of the \mathcal{L} -MFE method through numerical simulations. We envision that our work will provide a general framework for future theoretical work into incorporating Lindblad dynamics into more accurate semiclassical and mixed quantum-classical approaches.^{8,41–46}

II. THEORETICAL BACKGROUND

In order to clearly understand the assumptions underpinning the method that incorporates Lindblad dynamics into MFE, and to give a framework for deriving similar methods for other semiclassical approaches, we discuss the theoretical background of the Lindblad master equation, the MFE approach, and their combination in the density matrix form.

The total Hamiltonian of a system plus its environment can be written as

$$\hat{H}_T = \hat{H}_S \otimes \hat{\mathcal{I}}_E + \hat{\mathcal{I}}_S \otimes \hat{H}_E + \hat{H}_I, \quad (1)$$

where \hat{H}_S is the system Hamiltonian, $\hat{\mathcal{I}}_S$ is the identity in the system Hilbert space \mathcal{H}_S , \hat{H}_E is the environment Hamiltonian, $\hat{\mathcal{I}}_E$ is the identity in the environment Hilbert space \mathcal{H}_E , and \hat{H}_I is the interaction Hamiltonian between the system and the environment. Note that the partitioning of the system and environment is not unique. Any part of the total system that we do not want to explicitly simulate¹⁰ or is difficult to simulate can be treated as the environment.¹⁸

The time evolution of the density matrix $\hat{\rho}_T$ describing a quantum state of the entire system plus the environment is governed by the following quantum Liouville equation

$$\frac{d\hat{\rho}_T}{dt} \equiv \mathcal{L}_T[\hat{\rho}_T] = -\frac{i}{\hbar} [\hat{H}_T, \hat{\rho}_T], \quad (2)$$

where $\mathcal{L}_T[\cdot]$ is the Liouvillian superoperator that acts on operators and $[\cdot, \cdot]$ is the commutator between two operators.

When the quantum system of interest interacts with a large environment, the dynamics of the composite system and environment is generally too complicated and computationally expensive to keep track of in full detail. Instead, the dynamics of the system alone can be tracked using the reduced density matrix $\hat{\rho}_S$ (associated with \hat{H}_S in Eq. 1) defined as follows

$$\hat{\rho}_S(t) = \text{Tr}_E[\hat{\rho}_T(t)], \quad (3)$$

where $\text{Tr}_E[\hat{\rho}_T(t)] = \sum_i \langle i_E | \hat{\rho}_T(t) | i_E \rangle$ is the partial trace over the Hilbert space of the environment with basis $\{|i_E\rangle\}$.

For a closed quantum system (isolated system) with no entanglement or interaction with the environment ($\hat{H}_I = 0$ in Eq. 1), the total density matrix can be factorized as $\hat{\rho}_T = \hat{\rho}_S \otimes \hat{\rho}_E$ and the quantum Liouville equation for the reduced density matrix of the system is expressed as

$$\frac{d\hat{\rho}_S}{dt} = -\frac{i}{\hbar} [\hat{H}_S, \hat{\rho}_S]. \quad (4)$$

Likewise, the reduced density matrix of the environment $\hat{\rho}_E$ for a closed quantum system also satisfies its own quantum Liouville equation as $d\hat{\rho}_E/dt = -\frac{i}{\hbar} [\hat{H}_E, \hat{\rho}_E]$.

When there are explicit system-environment interactions ($\hat{H}_I \neq 0$), however, the dynamics of the reduced density matrix of the system $\hat{\rho}_S(t)$ can no longer be described by the unitary evolution of Eq. 4. An exact calculation of $\hat{\rho}_S(t)$ could be performed using Eq. 3 if $\hat{\rho}_T(t)$ is fully known, but this is generally infeasible to obtain due to the large number of environmental DOFs. Approximations of the environment and system-environment interactions can be made to calculate $\hat{\rho}_S(t)$ under certain conditions.

In situations where there are many system DOFs, further approximations must be made to calculate $\hat{\rho}_S(t)$. A common approach when there are several nuclear DOFs present in a molecular system is to separate the system into a classical subsystem and a quantum subsystem. The corresponding system Hamiltonian \hat{H}_S in this case is

$$\hat{H}_S = \hat{\mathcal{I}}_Q \otimes \hat{H}_C + \hat{H}_Q \otimes \hat{\mathcal{I}}_C + \hat{H}_{QC}, \quad (5)$$

where the quantum subsystem belonging to the Hilbert space \mathcal{H}_Q , with Hamiltonian \hat{H}_Q and identity $\hat{\mathcal{I}}_Q$, and the classical subsystem (typically nuclear DOF) belonging to the Hilbert space \mathcal{H}_C , with Hamiltonian \hat{H}_C and identity $\hat{\mathcal{I}}_C$, interact through \hat{H}_{QC} . In reactive molecular systems, the Hamiltonian \hat{H}_C is usually anharmonic and cannot easily be directly considered as \hat{H}_E . When possible, the system dynamics of Eq. 5 can be evaluated fully quantum mechanically; however, when the classical subsystem is too large, the semiclassical approximation can be made. Under the semiclassical approximation, the classical subsystem evolves using classical mechanics while the quantum subsystem evolves using quantum mechanics.

For molecular quantum dynamics, we consider the model system Hamiltonian that contains diabatic electronic states $\{|\psi_a\rangle\}$ (defining the quantum subsystem Hilbert space \mathcal{H}_Q) and nuclear DOFs \mathbf{R} (defining the classical subsystem Hilbert space \mathcal{H}_C) with the following form

$$\begin{aligned} \hat{H}_S = & \hat{\mathcal{I}}_Q \otimes \hat{\mathbf{T}}_{\mathbf{R}} + \hat{\mathcal{I}}_Q \otimes U_0(\hat{\mathbf{R}}) + \sum_{a,b} \varepsilon_{ab} |\psi_a\rangle \langle \psi_b| \otimes \hat{\mathcal{I}}_C \\ & + \sum_{a,b} |\psi_a\rangle \langle \psi_b| \otimes V_{ab}(\hat{\mathbf{R}}), \end{aligned} \quad (6)$$

where $\hat{\mathbf{T}}_{\mathbf{R}}$ is the kinetic energy of the nuclear DOFs, $U_0(\hat{\mathbf{R}})$ is the state independent potential, $\varepsilon_{ab} = \langle \psi_a | \hat{H}_Q | \psi_b \rangle$ is a matrix element of the diabatic quantum subsystem Hamiltonian, and $V_{ab}(\hat{\mathbf{R}}) = \langle \psi_a | \hat{H}_{QC} | \psi_b \rangle$ is a state dependent potential. Thus, in this model, we have

$$\hat{H}_C = \hat{\mathbf{T}}_{\mathbf{R}} + U_0(\hat{\mathbf{R}}), \quad (7a)$$

$$\hat{H}_Q = \sum_{a,b} \varepsilon_{ab} |\psi_a\rangle \langle \psi_b|, \quad (7b)$$

$$\hat{H}_{QC} = \sum_{a,b} |\psi_a\rangle \langle \psi_b| \otimes V_{ab}(\hat{\mathbf{R}}). \quad (7c)$$

Note that the theoretical approach described here is not limited to diabatic states. Additionally, the quantum subspace may include photonic degrees of freedom, as is the case for systems with polaritons.

The reduced density matrix of the quantum subsystem can be formally evaluated as

$$\hat{\rho}(t) = \text{Tr}_C[\hat{\rho}_S(t)], \quad (8)$$

where the trace is performed over the classical nuclear DOFs \mathbf{R} (or whatever the classical DOFs happen to be). When the mixed quantum-classical approximation is used,¹ the nuclear coordinates evolve classically and the quantum subsystem evolves using the time-dependent Schrödinger equation governed by $\hat{H}_Q + \hat{H}_{QC}(\mathbf{R})$. In this case, since only states in the quantum subspace are evolved using quantum mechanics, $\hat{\rho}(t)$ can be computationally evaluated without performing a trace on the much larger system Hilbert space which greatly improves computational efficiency.

A. Lindblad Jump Operator Dynamics

The Lindblad master equation^{31,32,47-51} is the most general Markovian description of a system density matrix $\hat{\rho}_S(t)$ interacting with the environment. It forms a dynamical semigroup of reduced density matrices that are trace-preserving (norm-preserving) and completely positive for population. The Lindblad master equation is expressed as

$$\begin{aligned} \frac{d\hat{\rho}_S}{dt} = & -\frac{i}{\hbar} [\hat{H}_S, \hat{\rho}_S] + \sum_k \Gamma_k \left(\hat{L}_k \hat{\rho}_S \hat{L}_k^\dagger - \frac{1}{2} \{ \hat{L}_k^\dagger \hat{L}_k, \hat{\rho}_S \} \right) \\ \equiv & \mathcal{L}_{\hat{H}} [\hat{\rho}_S] + \sum_k \mathcal{L}_{\hat{L}_k} [\hat{\rho}_S], \end{aligned} \quad (9)$$

where \hat{L}_k is a Lindblad jump operator that imparts the impact of the environment onto the system with interaction strength Γ_k (with a unit of rate or inverse time) and $\{\hat{A}, \hat{B}\} = \hat{A}\hat{B} + \hat{B}\hat{A}$ represents the anti-commutator. The superoperator $\mathcal{L}_{\hat{H}}[\cdot]$ is the part of the Liouvillian that describes the Hermitian dynamics of the system governed by \hat{H}_S defined as

$$\mathcal{L}_{\hat{H}}[\hat{\rho}_S] = -\frac{i}{\hbar} [\hat{H}_S, \hat{\rho}_S], \quad (10)$$

and $\mathcal{L}_{\hat{L}_k}[\cdot]$ is the part of the Liouvillian that describes the non-Hermitian Lindbladian dynamics associated with jump operator \hat{L}_k

$$\mathcal{L}_{\hat{L}_k}[\hat{\rho}_S] = \Gamma_k \left(\hat{L}_k \hat{\rho}_S \hat{L}_k^\dagger - \frac{1}{2} \{ \hat{L}_k^\dagger \hat{L}_k, \hat{\rho}_S \} \right), \quad (11)$$

governed by the approximations of \hat{H}_E and \hat{H}_I during the derivation of the Lindblad master equation.³¹ The sum $\sum_k \mathcal{L}_{\hat{L}_k}[\hat{\rho}_S]$ is sometimes referred to as the ‘‘dissipator’’. The Lindblad master equation provides a dynamical map

for $\hat{\rho}_S$ that forms a dynamical semigroup with generator $\mathcal{L}_{\hat{H}} + \sum_k \mathcal{L}_{\hat{L}_k}$. The Lindblad master equation in Eq. 9 can also be derived through the full quantum dynamics of \hat{H}_T by assuming weak system-environment interactions, the Born-Markov approximation, and the secular approximation.

In this work, we consider only a *single* decay channel characterized by the jump operator \hat{L}_S in the system Hilbert space \mathcal{H}_S (which the system Hamiltonian $\hat{H}_S = \hat{H}_C + \hat{H}_Q + \hat{H}_{QC}$ belongs to), and interaction strength Γ . This leads to the Lindblad master equation as follows

$$\frac{d\hat{\rho}_S}{dt} = -\frac{i}{\hbar} [\hat{H}_S, \hat{\rho}_S] + \Gamma \left(\hat{L}_S \hat{\rho}_S \hat{L}_S^\dagger - \frac{1}{2} \left\{ \hat{L}_S^\dagger \hat{L}_S, \hat{\rho}_S \right\} \right). \quad (12)$$

One of the most commonly used jump operators corresponds to a transition from one state to another state in the quantum subsystem. For example, for a transition from state $|\psi_1\rangle$ of the quantum subsystem to state $|\psi_0\rangle$ of the quantum subsystem with interaction strength Γ , the system Lindblad jump operator is

$$\hat{L}_S = |\psi_0\rangle\langle\psi_1| \otimes \hat{I}_C = \hat{L} \otimes \hat{I}_C, \quad (13)$$

and the jump operator \hat{L} only acts on the quantum DOFs in the subspace \mathcal{H}_Q . The above jump operator corresponds to a transition in the quantum subspace \mathcal{H}_Q with no impact on the classical (such as nuclear) subspace \mathcal{H}_C . We can represent this jump operator \hat{L}_S as well as the system Hamiltonian \hat{H}_S in a convenient basis $|\psi_a\rangle \otimes |\chi_\nu\rangle$, where $|\psi_a\rangle$ is the diabatic basis for the quantum subsystem and $|\chi_\nu\rangle$ is the discrete variable representation (DVR) basis for the classical subsystem.

B. Mean-Field Ehrenfest Approach

The mean-field Ehrenfest (MFE) approach is a semi-classical, mixed quantum-classical dynamics approach that simultaneously evolves a quantum subsystem and a classical subsystem. Multiple classical trajectories are evolved such that their distribution through time can be tracked to estimate e.g. the time evolution of the probability density of the wavefunction that the classical subsystem is approximating. For the electronic-nuclear dynamics of molecules, the electrons (or electrons and photons) are treated quantum mechanically while the nuclei are treated classically such that the distribution of the classical nuclear trajectories estimates the probability density of the nuclear wavefunction through time. The trajectory average of the electronic wavefunction is used to compute quantum estimators such as the elements of the electronic density matrix.

The MFE approach treats the electronic-nuclear dynamics such that each nuclear trajectory has a corresponding electronic wavefunction assigned to it. The nuclear coordinates parameterize the electronic Hamiltonian which evolves the electronic wavefunction at each

time step, while the coefficients of the electronic wavefunction generate a mean-field potential that exerts a classical force on the corresponding nuclear trajectory at each time step.

For the Hamiltonian \hat{H}_S (Eq. 5), the time dependent quantum state vector in the diabatic representation is expressed as

$$|\Psi_\xi(t)\rangle = \sum_a c_{a,\xi}(t) |\psi_a\rangle, \quad (14)$$

where $\{|\psi_a\rangle\}$ is a diabatic basis (not \mathbf{R} -dependent), and $\{c_{a,\xi}\}$ are expansion coefficients associated with the ξ th nuclear trajectory $\mathbf{R}_\xi(t)$. Note that the label of ξ inside $|\Psi_\xi(t)\rangle$ indicates its dependence on trajectory $\mathbf{R}_\xi(t)$. The trajectory-dependent equation of motion of the coefficient is

$$\frac{d}{dt} c_{a,\xi} = -\frac{i}{\hbar} \sum_b \left(V_{ab}(\mathbf{R}_\xi) + \varepsilon_{ab} \right) \cdot c_{b,\xi}, \quad (15)$$

where $V_{ab}(\mathbf{R}_\xi) = \langle\psi_a|\hat{H}_{QC}(\mathbf{R}_\xi)|\psi_b\rangle$ is a matrix element of the quantum-classical interaction Hamiltonian parameterized by the nuclear coordinates $\mathbf{R}_\xi(t)$, and ε_{ab} is a matrix element of \hat{H}_Q . The nuclear force in the diabatic representation is expressed as

$$\mathbf{F}_\xi = -\sum_{a,b} c_{a,\xi} \nabla_{\mathbf{R}} V_{ab}(\mathbf{R}_\xi) c_{b,\xi}^*, \quad (16)$$

and the nuclear coordinates evolve according to classical equations of motion with the above force. More details on the derivation and implementation of the MFE approach can be found in the literature.^{6,52–55}

The MFE approach can also be equivalently written down in terms of the reduced density matrix of the quantum subsystem (Eq. 8) as follows

$$\frac{d}{dt} \hat{\rho}_\xi = -\frac{i}{\hbar} \left[\hat{H}_Q + \hat{H}_{QC}(\mathbf{R}_\xi), \hat{\rho}_\xi \right], \quad (17)$$

where $\hat{\rho}_\xi$ is the reduced density matrix operator in the quantum subspace (defined in Eq. 8) associated with the ξ th independent nuclear trajectory $\mathbf{R}_\xi(t)$. More explicitly, the MFE reduced density matrix EOM and nuclear force are

$$\frac{d}{dt} \rho_{ab,\xi} = -\frac{i}{\hbar} \sum_c \left((V_{ac}(\mathbf{R}_\xi) + \varepsilon_{ac}) \rho_{cb,\xi} - \rho_{ac,\xi} (V_{cb}(\mathbf{R}_\xi) + \varepsilon_{cb}) \right), \quad (18)$$

$$\mathbf{F}_\xi = -\sum_{a,b} \rho_{ab,\xi} \nabla_{\mathbf{R}} V_{ab}(\mathbf{R}_\xi). \quad (19)$$

The estimator of the reduced density matrix elements $\rho_{ab}(t) = \langle\psi_a|\hat{\rho}(t)|\psi_b\rangle$ can be evaluated through averaging the Ehrenfest trajectories as follows

$$\rho_{ab}(t) = \frac{1}{N} \sum_{\xi=1}^N \rho_{ab,\xi}(t), \quad (20)$$

where N is the total number of trajectories used in the MQC description.

C. Ehrenfest Approach Combined with Lindblad Dynamics

When the nuclear DOFs \mathbf{R} are treated as classical DOFs under the mixed quantum-classical approximation (through independent trajectories $\mathbf{R}(t)$ instead of basis $\{|\chi_\nu\rangle\}$), the Lindblad master equation can still be used to describe the evolution of the quantum subsystem of $\hat{\rho}$ under the MFE approximation as follows

$$\frac{d\hat{\rho}}{dt} = -\frac{i}{\hbar} \left[\hat{H}_Q + \hat{H}_{QC}(\mathbf{R}), \hat{\rho} \right] + \mathcal{L}_{\hat{L}}[\hat{\rho}], \quad (21)$$

where the motion of \mathbf{R} is governed by the specific mixed quantum-classical approximation (governed by the mean-field force in Eq. 19 for MFE), and the Lindblad superoperator $\mathcal{L}_{\hat{L}}[\cdot]$ applied in the *quantum subspace* \mathcal{H}_Q is expressed as follows

$$\mathcal{L}_{\hat{L}}[\hat{\rho}] = \Gamma \cdot \left(\hat{L}\hat{\rho}\hat{L}^\dagger - \frac{1}{2} \left\{ \hat{L}^\dagger\hat{L}, \hat{\rho} \right\} \right). \quad (22)$$

Eq. 21 can be viewed as taking the mixed quantum-classical approximation on $-\frac{i}{\hbar}[\hat{H}_S, \hat{\rho}_S]$ in Eq. 12 then tracing out the classical DOFs \mathbf{R} . Eq. 21 can be viewed as a special case of the recently developed density matrix hybrid method¹⁸⁻²⁰ that combines MQC methods and master equation approaches, where the master equation is chosen to be Lindblad dynamics.

The single jump operator that we consider in this paper is the one that causes transitions from state $|1\rangle$ to state $|0\rangle$ (of the quantum subsystem \mathcal{H}_Q) as

$$\hat{L} = |\psi_0\rangle\langle\psi_1| \equiv |0\rangle\langle 1|, \quad (23)$$

where the corresponding system jump operator \hat{L}_S (in the system Hilbert space \mathcal{H}_S) is expressed in Eq. 13. The corresponding superoperator that describes the Lindbladian jump dynamics (based on Eq. 22) acting on the reduced density matrix of the quantum subsystem is then

$$\mathcal{L}_{\hat{L}}[\hat{\rho}] = \begin{bmatrix} \Gamma\rho_{11} & -\frac{\Gamma}{2}\rho_{01} & 0 & 0 & & \\ -\frac{\Gamma}{2}\rho_{10} & -\Gamma\rho_{11} & -\frac{\Gamma}{2}\rho_{12} & -\frac{\Gamma}{2}\rho_{13} & \dots & \\ 0 & -\frac{\Gamma}{2}\rho_{21} & 0 & 0 & & \\ 0 & -\frac{\Gamma}{2}\rho_{31} & 0 & 0 & & \\ & \vdots & & & & \ddots \end{bmatrix}. \quad (24)$$

From Eq. 24, it can be seen that the jump operator $\hat{L} = |0\rangle\langle 1|$ causes the population of state $|1\rangle$ to decay with a rate of Γ , state $|0\rangle$ to gain the population lost by state $|1\rangle$, and state $|1\rangle$ to decohere from every other state with a rate of $\frac{\Gamma}{2}$. This is an important feature of the Lindblad dynamics.

To better understand the dynamical picture, it is convenient to look at the superoperator acting on the reduced density matrix of only states $|0\rangle$ and $|1\rangle$ as follows

$$\mathcal{L}_{\hat{L}} \begin{bmatrix} \rho_{00} & \rho_{01} \\ \rho_{10} & \rho_{11} \end{bmatrix} = \begin{bmatrix} \Gamma\rho_{11} & -\frac{\Gamma}{2}\rho_{01} \\ -\frac{\Gamma}{2}\rho_{10} & -\Gamma\rho_{11} \end{bmatrix}. \quad (25)$$

In this simplified picture, considering state $|1\rangle$ to be the excited state and state $|0\rangle$ to be the ground state, the jump operator $\hat{L} = |0\rangle\langle 1|$ causes the excited state to decay to the ground state and both excited and ground states to decohere from each other. When $\hat{H}_Q = \hat{H}_{QC} = 0$ and no other jump operators have non-zero interaction strength, the time evolution of the reduced density matrix (in Eq. 25) can be analytically expressed as

$$e^{\mathcal{L}_{\hat{L}}t} \begin{bmatrix} \rho_{00} & \rho_{01} \\ \rho_{10} & \rho_{11} \end{bmatrix} = \begin{bmatrix} \rho_{00} + (1 - e^{-\Gamma t})\rho_{11} & e^{-\Gamma t/2}\rho_{01} \\ e^{-\Gamma t/2}\rho_{10} & e^{-\Gamma t}\rho_{11} \end{bmatrix}. \quad (26)$$

From Eq. 26, it can be seen that the jump operator $\hat{L} = |0\rangle\langle 1|$ causes exponential decay of the excited state to the ground state with a rate of Γ and exponential decay of the excited-ground coherence with a rate of $\Gamma/2$. This dynamical picture approximately corresponds to many physical phenomena such as spontaneous emission^{10,11} and photonic cavity loss when a single decay channel dominates.^{14,15}

Expressing the MFE approach in the density matrix form¹⁸⁻²⁰ (Eq. 17) allows for Lindblad dynamics to be implemented in a straightforward manner. This involves performing MFE dynamics in the Liouville space where each element $|\psi_a\rangle\langle\psi_b|$ is now treated as a basis vector. Eq. 19 and Eq. 21 describe the nuclear force and equation of motion of the density matrix elements, respectively. However, this density matrix formalism of MFE requires \mathcal{K}^2 density matrix elements to be dynamically updated for a dimension \mathcal{K} of the original quantum subsystem Hilbert space \mathcal{H}_Q , with a formal scaling in the range of $N \cdot \mathcal{K}^3$ to $N \cdot \mathcal{K}^4$ in terms of computational cost,³³ where N is the number of trajectories used to perform the MFE part of the Liouvillian in Eq. 21. The coefficient formalism MFE (Eq. 14), on the other hand, only requires \mathcal{K} coefficients to be dynamically updated, with a formal cost of $N \cdot \mathcal{K}^2$. Due to the numerically favorable scaling of a wavefunction based approach, together with the consideration that the trajectory average is required anyway in performing the MQC dynamics governed by Eq. 15, we choose to incorporate Lindblad dynamics into the regular coefficient-based approach of MFE. This requires a formulation of Lindblad dynamics in a coefficient-based formalism, which is derived in the next section.

III. THEORETICAL APPROACH

A. Trajectory-Based Solution of Lindblad Dynamics in the Hilbert Space

Consider the following short time propagation, from t to $t + dt$, of the reduced density operator $\hat{\rho}$ (Eq. 8) of a $\mathcal{K} \geq 2$ level system evolving under the dynamics of the quantum subsystem Hamiltonian $\hat{H} = \hat{H}_Q + \hat{H}_{QC}(\mathbf{R})$ and a single non-zero Lindblad jump operator $\hat{L} = |0\rangle\langle 1|$. For a small dt , the time evolution can be approximated as

$$\hat{\rho}(t + dt) = e^{\mathcal{L}dt}[\hat{\rho}(t)] \approx e^{\mathcal{L}_{\hat{H}}dt} e^{\mathcal{L}_{\hat{L}}dt}[\hat{\rho}(t)], \quad (27)$$

such that the jump operator evolution is applied separately from the Hamiltonian evolution.

The dynamics of the reduced density matrix elements in the subspace of $\{|0\rangle, |1\rangle\}$, governed by the jump operator \hat{L} (as described in Eq. 26), are expressed as follows

$$\rho_{11}(t+dt) = e^{-\Gamma dt} \rho_{11}(t), \quad (28a)$$

$$\rho_{00}(t+dt) = \rho_{00}(t) + (1 - e^{-\Gamma dt}) \rho_{11}(t), \quad (28b)$$

$$\rho_{01}(t+dt) = e^{-\Gamma dt/2} \rho_{01}(t), \quad (28c)$$

$$\rho_{10}(t+dt) = e^{-\Gamma dt/2} \rho_{10}(t). \quad (28d)$$

Further, for the coherences that involve states $|j\rangle \notin \{|0\rangle, |1\rangle\}$ due to the influence of the jump operator \hat{L} , the following equations hold

$$\rho_{j1}(t+dt) = e^{-\Gamma dt/2} \rho_{j1}(t), \quad (29a)$$

$$\rho_{1j}(t+dt) = e^{-\Gamma dt/2} \rho_{1j}(t), \quad (29b)$$

$$\rho_{j0}(t+dt) = \rho_{j0}(t), \quad (29c)$$

$$\rho_{0j}(t+dt) = \rho_{0j}(t), \quad (29d)$$

due to the matrix elements of Eq. 24 that involve states $\{|j\rangle\}$. The equation of motion for the coefficients $\{c_{a,\xi}(t)\}$ governed by the evolution of $\hat{H}_Q + \hat{H}_{QC}$ (or $e^{\mathcal{L}\hat{H}dt}$ in Eq. 27) can be computed based on the simple MFE approach in Eq. 15. The rest of the derivation will be focused on updating the coefficients to match these jump operator dynamics, separate from any Hamiltonian dynamics (as Eq. 27 allows us to do).

In order to achieve the same Lindblad dynamics from a mixed quantum-classical method such as MFE, the coefficients c_1 and c_0 (and $\{c_j\}$) must be evolved in a way such that their time evolution corresponds to equations 28a through 29d. The density matrix elements of equations 28a through 29d cannot, however, be directly replaced with the usual products of the coefficients c_1 and c_0 (and $\{c_j\}$). This is because this density matrix, in general, represents a mixed quantum state due to the fact that Lindblad dynamics describe an interaction with an external environment. The density matrix of a mixed quantum state cannot, in general, be represented by the density matrix of a single pure state as $c_0|\psi_0\rangle + c_1|\psi_1\rangle$. Thus, alternative approaches must be used to perform the time evolution of c_1 and c_0 with a combined result that satisfies Eq. 28a through Eq. 29d.

To this end, we take advantage of the existing multiple trajectories that are already present in mixed quantum-classical or semiclassical methods. We propose to evolve multiple trajectories and use the trajectory average of the electronic coefficients of these trajectories to compute the reduced density matrix elements at each time step, with the estimator of the reduced density matrix elements evaluated as

$$\rho_{ab}(t) = \frac{1}{N} \sum_{\xi=1}^N \rho_{ab,\xi}(t) = \frac{1}{N} \sum_{\xi=1}^N c_{a,\xi}(t) c_{b,\xi}^*(t), \quad (30)$$

where $c_{a,\xi}$ and $c_{b,\xi}$ are the coefficients of states $|a\rangle$ and $|b\rangle$, respectively, for trajectory $\mathbf{R}_\xi(t)$.

In addition, we introduce *random variation* of the time evolved coefficients as

$$c_{a,\xi}(t+dt) = \eta_{a,\xi} \cdot c_{a,\xi}(t) \equiv e^{i\theta_{a,\xi}} \cdot \chi_{a,\xi} \cdot c_{a,\xi}(t), \quad (31)$$

where $\{\eta_{a,\xi}\}$ are random complex variables with a certain probability distribution yet to be determined, such that the expectation value of the estimator of the time evolved reduced density matrix elements will exactly correspond to Eqs. 28a-29d. Further, $\{\theta_{a,\xi}\}$ are the phases and $\{\chi_{a,\xi}\}$ are the magnitudes of the complex variables.

Thus, the estimator of the time evolved reduced density matrix elements is

$$\begin{aligned} \rho_{ab}(t+dt) &= \frac{1}{N} \sum_{\xi=1}^N c_{a,\xi}(t+dt) c_{b,\xi}^*(t+dt) \\ &= \frac{1}{N} \sum_{\xi=1}^N \eta_{a,\xi} \cdot c_{a,\xi}(t) \cdot \eta_{b,\xi}^* \cdot c_{b,\xi}^*(t). \end{aligned} \quad (32)$$

To determine the detailed properties of the random variables $\{\eta_{a,\xi}\}$, we calculate the expectation value of functions of these random variables over their probability distribution $\mathcal{P}(\boldsymbol{\eta})$, such that a given function $f(\boldsymbol{\eta})$ has the following expectation value

$$\langle f(\boldsymbol{\eta}) \rangle = \int f(\boldsymbol{\eta}) \mathcal{P}(\boldsymbol{\eta}) d\boldsymbol{\eta}, \quad (33)$$

where $\mathcal{P}(\boldsymbol{\eta})$ is the joint probability distribution of all random variables $\boldsymbol{\eta}$.

Performing the above expectation value on Eq. 32, we have

$$\langle \rho_{ab}(t+dt) \rangle = \left\langle \frac{1}{N} \sum_{\xi=1}^N c_{a,\xi}(t+dt) c_{b,\xi}^*(t+dt) \right\rangle. \quad (34)$$

Under the converging limit where the number of trajectories tends to infinity, the estimator of the time evolved reduced density matrix elements equals its expectation value as follows

$$\lim_{N \rightarrow \infty} \rho_{ab}(t+dt) = \lim_{N \rightarrow \infty} \langle \rho_{ab}(t+dt) \rangle. \quad (35)$$

Thus, we propose to relate the estimator $\rho_{ab}(t+dt)$ in Eq. 34 and the estimator $\rho_{ab}(t)$ in Eq. 30 through Lindblad dynamics (Eqs. 28a-29d), such that

$$\langle \rho_{ab}(t+dt) \rangle = e^{\mathcal{L}_L dt} [\hat{\rho}(t)]_{ab}, \quad (36)$$

where $e^{\mathcal{L}_L dt} [\hat{\rho}(t)]$ generates the Lindblad jump dynamics found in Eqs. 28a-29d.

To this end, we establish the following equations to

govern the time evolution of the coefficients

$$\left\langle \frac{1}{N} \sum_{\xi=1}^N |c_{1,\xi}(t+dt)|^2 \right\rangle = e^{-\Gamma dt} \frac{1}{N} \sum_{\xi=1}^N |c_{1,\xi}(t)|^2, \quad (37a)$$

$$\begin{aligned} \left\langle \frac{1}{N} \sum_{\xi=1}^N |c_{0,\xi}(t+dt)|^2 \right\rangle & \quad (37b) \\ &= \frac{1}{N} \sum_{\xi=1}^N |c_{0,\xi}(t)|^2 + (1 - e^{-\Gamma dt}) \frac{1}{N} \sum_{\xi=1}^N |c_{1,\xi}(t)|^2, \end{aligned}$$

$$\begin{aligned} \left\langle \frac{1}{N} \sum_{\xi=1}^N c_{0,\xi}(t+dt) c_{1,\xi}^*(t+dt) \right\rangle & \quad (37c) \\ &= e^{-\Gamma dt/2} \frac{1}{N} \sum_{\xi=1}^N c_{0,\xi}(t) c_{1,\xi}^*(t), \end{aligned}$$

which match Eqs. 28a-28d. For states $|j\rangle \notin \{|0\rangle, |1\rangle\}$, we propose that

$$\begin{aligned} \left\langle \frac{1}{N} \sum_{\xi=1}^N c_{j,\xi}(t+dt) c_{1,\xi}^*(t+dt) \right\rangle & \quad (38a) \\ &= e^{-\Gamma dt/2} \frac{1}{N} \sum_{\xi=1}^N c_{j,\xi}(t) c_{1,\xi}^*(t), \end{aligned}$$

$$\left\langle \frac{1}{N} \sum_{\xi=1}^N c_{j,\xi}(t+dt) c_{0,\xi}^*(t+dt) \right\rangle = \frac{1}{N} \sum_{\xi=1}^N c_{j,\xi}(t) c_{0,\xi}^*(t), \quad (38b)$$

which match Eqs. 29a-29d. For simplicity, we assume that the coefficients $\{c_{j,\xi}\}$ for $|j\rangle \notin \{|0\rangle, |1\rangle\}$ are not changed by the Lindbladian time evolution, such that

$$c_{j,\xi}(t+dt) = c_{j,\xi}(t), \quad (39)$$

and all of the decoherence dynamics in Eqs. 29a-29c will be governed by the changes in $c_{1,\xi}$ and $c_{0,\xi}$. Ultimately, Eq. 39 only makes the choice that no arbitrary global phase is added to all coefficients since any other modification to the $c_{j,\xi}$ coefficients, besides adding a global phase, would incorrectly alter some of the reduced density matrix elements involving the $\{|j\rangle\}$ states.

The time evolved coefficients $c_{1,\xi}(t+dt)$ and $c_{0,\xi}(t+dt)$, based on Eq. 31, can be written as a product of the initial coefficient times a complex number

$$c_{1,\xi}(t+dt) = e^{i\theta_{1,\xi}} \chi_{1,\xi} c_{1,\xi}(t), \quad \chi_{1,\xi} \geq 0 \quad (40a)$$

$$c_{0,\xi}(t+dt) = e^{i\theta_{0,\xi}} \chi_{0,\xi} c_{0,\xi}(t), \quad \chi_{0,\xi} \geq 0 \quad (40b)$$

where $\theta_{1,\xi}$ and $\theta_{0,\xi}$ are (potentially random) phases and $\chi_{1,\xi}$ and $\chi_{0,\xi}$ are (potentially random) magnitudes. For the special case that $c_{l,\xi}(t) = 0$ and $c_{l,\xi}(t+dt) \neq 0$, $l \in \{0, 1\}$, the magnitude $\chi_{l,\xi}$ can be written as some finite magnitude divided by $c_{l,\xi}(t)$ such that $c_{l,\xi}(t+dt)$ is non-zero and well defined.

When $\Gamma dt = 0$, the density matrices do not change from one time step to another. Accordingly, when $\Gamma dt = 0$, the coefficients of the trajectories $c_{1,\xi}$ and $c_{0,\xi}$ should not change. Thus, we add a constraint to the coefficient evolution as follows

$$\lim_{\Gamma dt \rightarrow 0} e^{i\theta_{1,\xi}} \chi_{1,\xi} = 1, \quad (41a)$$

$$\lim_{\Gamma dt \rightarrow 0} e^{i\theta_{0,\xi}} \chi_{0,\xi} = 1. \quad (41b)$$

While there are several possible choices for constructing $c_{1,\xi}(t+dt)$ and $c_{0,\xi}(t+dt)$ that agree with Eqs. 37a-41b, it is important to consider how these choices affect the Hamiltonian dynamics (evolved by $e^{\mathcal{L}_{\hat{H}} dt}$) that occur in conjunction with the Lindblad dynamics. Certain choices of $c_{1,\xi}(t+dt)$ and $c_{0,\xi}(t+dt)$ may cause the Hamiltonian dynamics to diverge from the results of the exact Liouvillian dynamics, for example, when they do not conserve the trace of the density matrix within a trajectory. To avoid this, we add on an additional constraint to the coefficient evolution that

$$|c_{1,\xi}(t+dt)|^2 + |c_{0,\xi}(t+dt)|^2 = |c_{1,\xi}(t)|^2 + |c_{0,\xi}(t)|^2, \quad (42)$$

such that the trace of the density matrix of each trajectory is conserved. Eq. 42 can be rearranged and combined with Eq. 40a, resulting in the following equation

$$\begin{aligned} |c_{0,\xi}(t+dt)|^2 & \\ &= |c_{0,\xi}(t)|^2 \left(\frac{|c_{0,\xi}(t)|^2 + (1 - \chi_{1,\xi}^2) |c_{1,\xi}(t)|^2}{|c_{0,\xi}(t)|^2} \right), \end{aligned} \quad (43)$$

which can be further expressed as

$$\begin{aligned} c_{0,\xi}(t+dt) & \\ &= e^{i\theta_{0,\xi}} c_{0,\xi}(t) \sqrt{\frac{|c_{0,\xi}(t)|^2 + (1 - \chi_{1,\xi}^2) |c_{1,\xi}(t)|^2}{|c_{0,\xi}(t)|^2}} \\ &= e^{i\theta_{0,\xi}} c_{0,\xi}(t) \cdot \chi_{0,\xi}. \end{aligned} \quad (44)$$

From Eq. 44, it is now clear that the square root in the first line is the expression for $\chi_{0,\xi}$

$$\chi_{0,\xi} = \sqrt{\frac{|c_{0,\xi}(t)|^2 + (1 - \chi_{1,\xi}^2) |c_{1,\xi}(t)|^2}{|c_{0,\xi}(t)|^2}}. \quad (45)$$

To determine the values of the rest of unknown variables in Eq. 40a and Eq. 40b, we relate them to the right hand sides of Eqs. 37a-37c. To begin, the left hand side of Eq. 37a can be rewritten as

$$\left\langle \frac{1}{N} \sum_{\xi} |c_{1,\xi}(t+dt)|^2 \right\rangle = \frac{1}{N} \sum_{\xi} \left\langle |c_{1,\xi}(t+dt)|^2 \right\rangle, \quad (46)$$

due to the linearity of the expectation value (see Eq. 33). Taking the expectation value of Eq. 40a yields

$$\langle |c_{1,\xi}(t+dt)|^2 \rangle = \langle \chi_{1,\xi}^2 \rangle |c_{1,\xi}(t)|^2. \quad (47)$$

Plugging the above expression into the right hand side of Eq. 46 and relating this to the right hand side of Eq. 37a, we have

$$\frac{1}{N} \sum_{\xi} \langle \chi_{1,\xi}^2 \rangle |c_{1,\xi}(t)|^2 = \frac{1}{N} \sum_{\xi} e^{-\Gamma dt} |c_{1,\xi}(t)|^2. \quad (48)$$

To simplify the analysis, we use the following sufficient assumption that

$$\langle \chi_{1,\xi}^2 \rangle = e^{-\Gamma dt}, \quad (49)$$

such that Eq. 48 (and thus Eq. 37a) is satisfied. A similar analysis of the left hand side of Eq. 37b yields

$$\begin{aligned} \left\langle \frac{1}{N} \sum_{\xi} |c_{0,\xi}(t+dt)|^2 \right\rangle &= \frac{1}{N} \sum_{\xi} \langle |c_{0,\xi}(t+dt)|^2 \rangle \\ &= \frac{1}{N} \sum_{\xi} (|c_{0,\xi}(t)|^2 + (1 - \langle \chi_{1,\xi}^2 \rangle) |c_{1,\xi}(t)|^2) \\ &= \frac{1}{N} \sum_{\xi} |c_{0,\xi}(t)|^2 + (1 - e^{-\Gamma dt}) \frac{1}{N} \sum_{\xi} |c_{1,\xi}(t)|^2, \end{aligned} \quad (50)$$

where from the first line to the second line of the above equation, we used Eq. 43, and from the second line to the third line, we used Eq. 49. Note that the above equation automatically guarantees the requirement in Eq. 37b.

The left hand side of Eq. 37c can similarly be written as

$$\begin{aligned} \left\langle \frac{1}{N} \sum_{\xi} c_{0,\xi}(t+dt) c_{1,\xi}^*(t+dt) \right\rangle & \quad (51) \\ &= \frac{1}{N} \sum_{\xi} \langle c_{0,\xi}(t+dt) c_{1,\xi}^*(t+dt) \rangle, \end{aligned}$$

where the expectation value can be written as

$$\begin{aligned} \left\langle c_{0,\xi}(t+dt) c_{1,\xi}^*(t+dt) \right\rangle & \quad (52) \\ &= c_{0,\xi}(t) c_{1,\xi}^*(t) \\ &\quad \times \left\langle e^{i\theta_{\xi}} \chi_{1,\xi} \sqrt{\frac{|c_{0,\xi}(t)|^2 + (1 - \chi_{1,\xi}^2) |c_{1,\xi}(t)|^2}{|c_{0,\xi}(t)|^2}} \right\rangle, \end{aligned}$$

where $\theta_{\xi} = \theta_{0,\xi} - \theta_{1,\xi}$, and we have used the expression of $\chi_{0,\xi}$ in Eq. 45. The above expectation value can be

related to the right hand side of Eq. 37c as

$$\begin{aligned} \frac{1}{N} \sum_{\xi} c_{0,\xi}(t) c_{1,\xi}^*(t) & \quad (53) \\ &\times \left\langle e^{i\theta_{\xi}} \chi_{1,\xi} \sqrt{\frac{|c_{0,\xi}(t)|^2 + (1 - \chi_{1,\xi}^2) |c_{1,\xi}(t)|^2}{|c_{0,\xi}(t)|^2}} \right\rangle \\ &= \frac{1}{N} \sum_{\xi} c_{0,\xi}(t) c_{1,\xi}^*(t) e^{-\Gamma dt/2}. \end{aligned}$$

We make the assumption that

$$\left\langle e^{i\theta_{\xi}} \chi_{1,\xi} \sqrt{\frac{|c_{0,\xi}(t)|^2 + (1 - \chi_{1,\xi}^2) |c_{1,\xi}(t)|^2}{|c_{0,\xi}(t)|^2}} \right\rangle = e^{-\Gamma dt/2}, \quad (54)$$

such that Eq. 53 (and thus Eq. 37c) is satisfied.

Equations 49 and 54 govern how the (potentially random) variables θ_{ξ} and $\chi_{1,\xi}$ must be selected in order to obey equations 37a through 42. To avoid considering joint probability distributions of dependent random variables, we make the assumption that

$$\mathcal{P}(\theta_{\xi}, \chi_{1,\xi}) = \mathcal{P}(\theta_{\xi}) \cdot \mathcal{P}(\chi_{1,\xi}), \quad (55)$$

such that θ_{ξ} and $\chi_{1,\xi}$ are independent variables for distribution $\mathcal{P}(\eta)$. Thus, Eq. 54 can be written as

$$\begin{aligned} \langle e^{i\theta_{\xi}} \rangle \cdot \left\langle \chi_{1,\xi} \sqrt{\frac{|c_{0,\xi}(t)|^2 + (1 - \chi_{1,\xi}^2) |c_{1,\xi}(t)|^2}{|c_{0,\xi}(t)|^2}} \right\rangle & \\ = e^{-\Gamma dt/2}. & \quad (56) \end{aligned}$$

To further simplify the analysis by reducing the number of random variables, we make the assumption that

$$\langle \chi_{1,\xi} \rangle = \chi_{1,\xi}, \quad (57)$$

such that $\chi_{1,\xi}$ is a constant. Combining the above equation with Eq. 49 yields $\langle \chi_{1,\xi}^2 \rangle = \chi_{1,\xi}^2$, which means that

$$\chi_{1,\xi} = e^{-\Gamma dt/2}. \quad (58)$$

This expression of $\chi_{1,\xi}$ can be plugged into Eq. 56 to find

$$\langle e^{i\theta_{\xi}} \rangle = \frac{|c_{0,\xi}(t)|}{\sqrt{|c_{0,\xi}(t)|^2 + (1 - e^{-\Gamma dt}) |c_{1,\xi}(t)|^2}}. \quad (59)$$

The right hand side of Eq. 59 is purely real and is always within the range 0 to 1 for $\Gamma dt \geq 0$. Thus, there exist distributions of θ_{ξ} that satisfy the above equation because the expectation value of $e^{i\theta_{\xi}}$ can have a magnitude within the range 0 to 1. To reduce large jumps in these phase variables, we assume that

$$\mathcal{P}(\theta_{\xi}) = \frac{1}{2\Delta\theta_{\xi}}, \quad -\Delta\theta_{\xi} \leq \theta_{\xi} < \Delta\theta_{\xi}, \quad (60)$$

such that the probability distribution of the random phase θ_ξ follows a uniform distribution of width $2\Delta\theta_\xi$ centered around 0. The expectation value $\langle e^{i\theta_\xi} \rangle$ can thus be calculated based on the definition in Eq. 33, and combined with Eq. 59 to find

$$\frac{\sin(\Delta\theta_\xi)}{\Delta\theta_\xi} = \frac{|c_{0,\xi}(t)|}{\sqrt{|c_{0,\xi}(t)|^2 + (1 - e^{-\Gamma dt}) |c_{1,\xi}(t)|^2}}. \quad (61)$$

This means that choosing $\Delta\theta_\xi$ according to Eq. 61 as the bounds of the uniform probability distribution of θ_ξ will satisfy the expectation value relations in all previous equations. Since Eq. 61 is a transcendental equation, no general closed form exists for the solutions to $\Delta\theta_\xi$. To find $\Delta\theta_\xi$, a numerical interpolation function of the first positive solution of $\sin(x) = ax$ can be pre-computed for the values $0 \leq a \leq 1$ and then used during the simulation.

Up to this point, the only unspecified variables are the individual phases $\theta_{0,\xi}$ and $\theta_{1,\xi}$. To determine these variables, Eq. 38a and Eq. 38b can be used. Using the conditions outlined in Eq. 39 and Eq. 58, the left hand side of Eq. 38a can be rewritten as

$$\begin{aligned} \left\langle \frac{1}{N} \sum_{\xi} c_{j,\xi}(t+dt) c_{1,\xi}^*(t+dt) \right\rangle & \quad (62) \\ &= \frac{1}{N} \sum_{\xi} c_{j,\xi}(t) \langle e^{-i\theta_{1,\xi}} \rangle e^{-\Gamma dt/2} c_{1,\xi}^*(t), \end{aligned}$$

which can be related to the right hand side of Eq. 38a as

$$\begin{aligned} \frac{1}{N} \sum_{\xi} c_{j,\xi}(t) \langle e^{-i\theta_{1,\xi}} \rangle e^{-\Gamma dt/2} c_{1,\xi}^*(t) & \quad (63) \\ &= \frac{1}{N} \sum_{\xi} c_{j,\xi}(t) e^{-\Gamma dt/2} c_{1,\xi}^*(t). \end{aligned}$$

The sufficient assumption to make the above equation (hence Eq. 38a) valid is to require

$$\langle e^{-i\theta_{1,\xi}} \rangle = 1. \quad (64)$$

Since $\langle e^{-i\theta_{1,\xi}} \rangle$ can only be equal to 1 if every possible instance of $e^{-i\theta_{1,\xi}}$ is 1, it follows that

$$\theta_{1,\xi} = 0, \quad \theta_\xi = \theta_{0,\xi} - \theta_{1,\xi} = \theta_{0,\xi}, \quad (65)$$

such that only $c_{0,\xi}$ obtains a random phase governed by the distribution in Eq. 61, and $c_{1,\xi}$ does not. More specifically, Eq. 59 becomes

$$\langle e^{\pm i\theta_{0,\xi}} \rangle = \frac{|c_{0,\xi}(t)|}{\sqrt{|c_{0,\xi}(t)|^2 + (1 - e^{-\Gamma dt}) |c_{1,\xi}(t)|^2}}. \quad (66)$$

This means that using the information of how state $|1\rangle$ decoheres with other states $|j\rangle \notin \{|0\rangle, |1\rangle\}$ allows us to

determine how the random phase θ_ξ should be partitioned among $\theta_{0,\xi}$ and $\theta_{1,\xi}$. Eq. 64 suggests that there is no need to add additional random phase to coefficients $c_{1,\xi}(t)$ if one wants to correctly describe the decoherence dynamics between state $|1\rangle$ and $|j\rangle$ (for $j \neq 0, 1$) governed by Lindblad dynamics (Eq. 24). The information in Eq. 63 was omitted when developing the Ehrenfest+R method. Nevertheless, the same choice was empirically discovered through the use of numerical simulations of Ehrenfest+R.^{10,11}

Using a similar analysis of the above procedure for the left-hand side of Eq. 38b, together with Eq. 45 and Eq. 66, it follows that

$$\begin{aligned} \left\langle \frac{1}{N} \sum_{\xi} c_{j,\xi}(t+dt) c_{0,\xi}^*(t+dt) \right\rangle & \quad (67) \\ &= \frac{1}{N} \sum_{\xi} c_{j,\xi}(t) c_{0,\xi}^*(t) \langle e^{-i\theta_{0,\xi}} \rangle \langle \chi_{0,\xi} \rangle \\ &= \frac{1}{N} \sum_{\xi} c_{j,\xi}(t) c_{0,\xi}^*(t) \\ &\quad \times \frac{|c_{0,\xi}(t)|}{\sqrt{|c_{0,\xi}(t)|^2 + (1 - e^{-\Gamma dt}) |c_{1,\xi}(t)|^2}} \\ &\quad \times \frac{\sqrt{|c_{0,\xi}(t)|^2 + (1 - e^{-\Gamma dt}) |c_{1,\xi}(t)|^2}}{|c_{0,\xi}(t)|} \\ &= \frac{1}{N} \sum_{\xi} c_{j,\xi}(t) c_{0,\xi}^*(t), \quad (68) \end{aligned}$$

which guarantees the right hand side of Eq. 38b, thus the choice of $\theta_{1,\xi}$ and $\theta_{0,\xi}$ in Eq. 65 satisfies both equations 38a and 38b.

B. Summary of the \mathcal{L} -MFE Method

To summarize, we propose to incorporate Lindblad dynamics by adjusting the quantum expansion coefficients as follows

$$\hat{\mathcal{T}}(dt) \cdot c_{1,\xi}(t) \equiv c_{1,\xi}(t+dt) = e^{-\Gamma dt/2} c_{1,\xi}(t), \quad (69a)$$

$$\begin{aligned} \hat{\mathcal{T}}(dt) \cdot c_{0,\xi}(t) & \equiv c_{0,\xi}(t+dt) \\ &= e^{i\theta_\xi} e^{i\varphi_\xi^0} \sqrt{|c_{0,\xi}(t)|^2 + (1 - e^{-\Gamma dt}) |c_{1,\xi}(t)|^2}, \quad (69b) \end{aligned}$$

$$\hat{\mathcal{T}}(dt) \cdot c_{j,\xi}(t) \equiv c_{j,\xi}(t+dt) = c_{j,\xi}(t) \quad (\text{for } j \neq 0, 1), \quad (69c)$$

where $\hat{\mathcal{T}}(dt)$ is a *formal* transition operator that propagates the coefficients as designed, $e^{i\varphi_\xi^0} = c_{0,\xi}(t)/|c_{0,\xi}(t)|$ is the phase factor of $c_{0,\xi}(t)$, and the random phase θ_ξ is sampled based on a uniform distribution $\mathcal{P}(\theta_\xi)$ expressed

as

$$\mathcal{P}(\theta_\xi) = \frac{1}{2\Delta\theta_\xi}, \quad -\Delta\theta_\xi \leq \theta_\xi < \Delta\theta_\xi, \quad (70)$$

with the width $\Delta\theta_\xi$ determined from the following transcendental equation

$$\frac{\sin(\Delta\theta_\xi)}{\Delta\theta_\xi} = \frac{|c_{0,\xi}(t)|}{\sqrt{|c_{0,\xi}(t)|^2 + (1 - e^{-\Gamma dt})|c_{1,\xi}(t)|^2}}. \quad (71)$$

Thus, we explicitly use the trajectory average to converge to the expectation value defined in Eq. 33. This is one of the main theoretical results of the paper. Note that when $c_{0,\xi}(t) = 0$ and $c_{1,\xi}(t) \neq 0$, the random angle θ_ξ added to the ground state is sampled from $-\pi$ to π due to Eq. 71 which completely randomizes the phase of the ground state, which renders the undetermined phase factor $e^{i\varphi_\xi^0}$ irrelevant.

These effective Lindblad updates of the electronic coefficients described in Eqs. 69a-69c can be combined with the Ehrenfest part of the electronic coefficients update described in Eq. 15 and Eq. 16 to describe the mixed quantum-classical dynamics subject to a Lindblad type decay. We refer to this approach as the \mathcal{L} -MFE method for the remainder of the paper. The coefficient propagation of the \mathcal{L} -MFE method can be expressed as

$$\mathbf{c}(t+dt) = \hat{\mathcal{T}}(dt/2) \cdot e^{-\frac{i}{\hbar}(\hat{H}_Q + \hat{H}_{QC})dt} \cdot \hat{\mathcal{T}}(dt/2) \cdot \mathbf{c}(t), \quad (72)$$

where $\mathbf{c}(t)$ is the vector of the quantum coefficients, $\hat{\mathcal{T}}$ describes the coefficients update due to the jump operator using Eqs. 69a-69c, and $e^{-\frac{i}{\hbar}(\hat{H}_Q + \hat{H}_{QC})dt}$ describes the unitary evolution of the coefficients due the MFE dynamics described in Eq. 15. Note that $\hat{H}_{QC}(\mathbf{R})$ depends on the nuclear DOFs \mathbf{R} , where $\mathbf{R}(t)$ evolves based on the force in Eq. 16. Here, we use a symmetrical Trotter decomposition in Eq. 72 to reduce error due to a finite time step dt , and we put the Ehrenfest propagation in the middle because it is computational expensive (which scales as $\sim \mathcal{K}^2$) compared to the Lindblad decay part (denoted by $\hat{\mathcal{T}}$) which only requires the update of two coefficients $c_{1,\xi}(t)$ and $c_{0,\xi}(t)$.

The \mathcal{L} -MFE algorithm outlined in Eq. 72 will, in principle, generate different results compared to Eq. 21 where the Lindblad dynamics are propagated deterministically in the Liouville space. This is because the \mathcal{L} -MFE method adds random phases to state $|0\rangle$ (for the $\hat{L} = |0\rangle\langle 1|$ jump operator) through $\hat{\mathcal{T}}$ (see Eq. 69b) for each individual trajectory. Further, these random phases in $c_{0,\xi}(t)$ will also influence the magnitude of populations through coupling term $V_{01}(\mathbf{R}_\xi) + \varepsilon_{01}$. Thus, \mathcal{L} -MFE adds different phases onto $\rho_{01,\xi}$ (as well as on $\rho_{10,\xi}$) and generates different populations $\rho_{00,\xi}$ and $\rho_{11,\xi}$ for each individual trajectory. The $\mathcal{L}_{\hat{L}}[\hat{\rho}]$ term in Eq. 21, on the other hand, causes *deterministic* changes for the density matrix elements of all trajectories. Thus, the random phases in \mathcal{L} -MFE will influence the nuclear forces

in Eq. 19 and these different nuclear forces for each trajectory further influences the nuclear motion for \mathbf{R} , and eventually back influence the electronic dynamics through $e^{-\frac{i}{\hbar}(\hat{H}_Q + \hat{H}_{QC}(\mathbf{R}))dt}$ in Eq. 72. Future research will focus on investigating the difference between Eq. 21 and Eq. 72. Nevertheless, numerical results obtained for the model systems (Eqs. 76a-76h and Eq. 77) produce visually identical results using either Eq. 21 or Eq. 72.

C. Comparison with Other Stochastic Wavefunction Approaches

We want to emphasize the connections and differences between the current \mathcal{L} -MFE method and previous approaches that try to accomplish Lindblad dynamics through stochastic wavefunction approaches, such as Monte Carlo wave-function methods³⁵⁻³⁸ and the Ehrenfest+R approach.^{10-12,39,40}

The Monte Carlo wavefunction method^{35,36} expresses the stochastic time evolution of the system's wavefunction as follows^{34,56}

$$d|\psi_S(t)\rangle = -\frac{i}{\hbar}\hat{H}_{\text{eff}}|\psi_S(t)\rangle \cdot dt + \sum_k \left(\frac{\sqrt{\Gamma_k}\hat{L}_k}{\langle\psi_S(t)|\Gamma_k\hat{L}_k^\dagger\hat{L}_k|\psi_S(t)\rangle} - 1 \right) |\psi_S(t)\rangle \cdot dN_k, \quad (73)$$

where $\hat{H}_{\text{eff}} = \hat{H}_S - \frac{1}{2}\sum_k i\hbar\Gamma_k\hat{L}_k^\dagger\hat{L}_k$ is the effective Hamiltonian that captures the time evolution governed by \hat{H}_S and the $-\sum_k \Gamma_k \frac{1}{2}\{\hat{L}_k^\dagger\hat{L}_k, \hat{\rho}_S\}$ term that describes the population decays in Eq. 9. Further, the second term on the right hand side of Eq. 73 effectively captures the $\sum_k \Gamma_k \hat{L}_k \hat{\rho}_S \hat{L}_k^\dagger$ term in Eq. 9, with $dN_k = 0, 1$ and $\langle dN_k \rangle = \Gamma_k \langle \psi_S(t) | \hat{L}_k^\dagger \hat{L}_k | \psi_S(t) \rangle^2 dt$. This term performs a Poisson jump process that captures the projective action of the environment on the system that randomly collapses the system wavefunction into a pure system eigenstate. The trajectory average of Eq. 73 with a large number of realizations (jump trajectories) generates results identical to $\hat{\rho}_S(t)$ described by the Lindblad master equation in Eq. 9. The equivalence of these two descriptions can be viewed as the correspondence between the stochastic quantum state diffusion equation (Eq. 73) and the deterministic Wigner Fokker-Planck equation (which can be written in the Lindblad master equation form of Eq. 9).⁵⁷

The \mathcal{L} -MFE method, on the other hand, does not collapse trajectories onto a single system state, which avoids large changes in the magnitudes of the coefficients. Further, the change in magnitude of the coefficients is deterministic, whereas the magnitude of the coefficients in the Monte Carlo wavefunction method is stochastic. Further, the phases of the coefficients in \mathcal{L} -MFE only slightly vary between time steps with no large jumps. When explicitly considering $\hat{H}_C + \hat{H}_{QC}$, the stochastic Schrödinger equation approach can encounter numerical instabilities³⁸ due to large changes of the electronic coefficients, whereas the

\mathcal{L} -MFE approach provides a stable numerical integration of the equation of motion due to the small changes of phase in the coefficients. The \mathcal{L} -MFE approach, in addition, can be easily combined with *any* mixed quantum-classical or semiclassical approach.

The Ehrenfest+R method¹⁰ was originally developed to simulate the electronic quantum subsystem coupled to the classical electromagnetic field in order to accurately describes spontaneous emission processes. It effectively captures Lindblad dynamics with a deterministic change of the magnitude of the quantum coefficients, and stochastic changes of the phases. While the \mathcal{L} -MFE method is similar to (and largely inspired by) the Ehrenfest+R method, there is a key difference between Ehrenfest+R and \mathcal{L} -MFE in the off-diagonal reduced density matrix element decay procedure. To facilitate the theoretical comparison, we briefly summarize the Ehrenfest+R method¹⁰ in Appendix A.

The Ehrenfest+R approach was derived under the condition that $\Gamma \ll E$, where Γ is the decay rate of the jump operator \hat{L} and E is the energy difference between state $|0\rangle$ and $|1\rangle$ (see Appendix A). This condition is thus the regime where the Ehrenfest+R approach can be applied with guaranteed accuracy. The \mathcal{L} -MFE method, on the other hand, does not have any restrictions on the parameter regimes where it is applicable.

The “+R decay” procedure (see Eq. A24 through Eq. A28) in Ehrenfest+R was designed to correct the decay of the diagonal density matrix elements and off-diagonal elements independently, with the goal that the combined Ehrenfest dynamics and +R decay dynamics will match the Lindblad decay of the density matrix elements. However, the procedure to adjust the diagonals of the density matrix by changing the magnitudes of the corresponding coefficients also changes the off-diagonal density matrix elements, causing unintended deviations in the dynamics. The off-diagonal relaxation decay rate in Ehrenfest+R, which is proposed to be (see Eq. 53 in Ref. 10)

$$\gamma_R = \frac{\Gamma}{2} (1 - |c_{0,\xi}(t)|^2 + |c_{1,\xi}(t)|^2), \quad (74)$$

does not account for this effect, thus the corresponding dynamics do not fully capture those of Eqs. 28a through 29d.

To properly account for this effect, the γ_R rate in Ehrenfest+R should be modified to be

$$\begin{aligned} \gamma'_R &= \frac{\Gamma}{2} (1 - |c_{0,\xi}(t)|^2 + |c_{1,\xi}(t)|^2) \\ &+ \frac{1}{dt} \ln \left(\frac{|c_{0,\xi}(t+dt)c_{1,\xi}(t+dt)|}{|c_{0,\xi}(t)c_{1,\xi}(t)|} \right) \end{aligned} \quad (75)$$

for $|c_{0,\xi}(t)c_{1,\xi}(t)| \neq 0$. The detailed derivation of this expression is provided in Appendix B. The \mathcal{L} -MFE method already accounts for the effect that modifying the magnitudes of the coefficients has on the off-diagonals of the density matrix, as shown in Eq. 59. This is another main theoretical result of the current paper.

Additionally, in the Ehrenfest+R approach, it was numerically found that adding random phase only to $c_{0,\xi}(t+dt)$ gave the most accurate results;¹¹ however, these choices lacked a rigorous theoretical reason for why this should be the case and it was speculated that this is because spontaneous emission from states $|1\rangle$ to $|0\rangle$ should not affect the coherence of state $|1\rangle$ with other states $\{|j\rangle\}$. In contrast, the analysis in this paper shows that the mathematical reason for this choice of random phase lies in the fact that the excited state $|1\rangle$ decoheres with every other state of the quantum subsystem while state $|0\rangle$ only decoheres with state $|1\rangle$, when $\hat{L} = |0\rangle\langle 1|$. This fact is derived from applying the Lindbladian $\mathcal{L}_{\hat{L}}$ (with $\hat{L} = |0\rangle\langle 1|$) to the entire reduced density matrix of \mathcal{K} states instead of only the reduced density matrix of $|0\rangle$ and $|1\rangle$. While state $|1\rangle$ decoheres with every other state, the decoherence with states $\{|j\rangle\}$ is entirely captured by the reduction of the magnitude of $c_{1,\xi}(t+dt)$ by $e^{-\Gamma dt/2}$; thus, the phase of state $|1\rangle$ does not need to provide any additional decoherence. In contrast, state $|0\rangle$ does not decohere with states $\{|j\rangle\}$, but the increase of the magnitude of $c_{0,\xi}(t+dt)$ causes an increase in coherence with states $\{|j\rangle\}$. The role of the random phase applied to state $|0\rangle$, aside from adjusting the coherence with state $|1\rangle$, is to add decoherence to cancel out the increase in coherence with states $\{|j\rangle\}$ due to the increase of the magnitude of $c_{0,\xi}(t+dt)$.

Lastly, when $\hat{H}_{QC} + \hat{H}_C = 0$ (no nuclear DOFs present in the system Hamiltonian), the \mathcal{L} -MFE approach in Eq. 72 (or equivalently Eq. 21) provides identical results as those obtained by solving Eq. 12, regardless of the choice of dt (as long as it is small enough to provide a stable integration of $-\frac{i}{\hbar}[\hat{H}_Q, \hat{\rho}]$). This is because in the \mathcal{L} -MFE approach, the decay dynamics are designed to exactly match the analytical time evolution of the reduced density matrix elements. Consequentially, if the Hamiltonian is 0 and only jump operator dynamics are present, the choice of dt for \mathcal{L} -MFE could be arbitrarily large and still give the correct dynamics. On the other hand, under the same condition when $\hat{H}_{QC} + \hat{H}_C = 0$, the Ehrenfest+R approach is only accurate up to first order in dt (see Eq. A28 and Eq. B7).

IV. MODEL SYSTEMS AND COMPUTATIONAL DETAILS

Simple Model Systems. To assess the accuracy of the \mathcal{L} -MFE method, a variety of models are tested and compared with an exact calculation of the corresponding Lindblad dynamics. All of the following simple models are associated with a single Lindblad jump operator $\hat{L} = |0\rangle\langle 1|$ with interaction strength $\Gamma = 0.05$ a.u. These

models are

$$\text{Model 1: } \hat{H}_Q = \begin{bmatrix} 0 & 0 \\ 0 & 0 \end{bmatrix}, \quad |\Psi(0)\rangle = |1\rangle \quad (76a)$$

$$\text{Model 2: } \hat{H}_Q = \begin{bmatrix} 0 & 0 \\ 0 & 0 \end{bmatrix}, \quad |\Psi(0)\rangle = \frac{|0\rangle + |1\rangle}{\sqrt{2}} \quad (76b)$$

$$\text{Model 3: } \hat{H}_Q = \begin{bmatrix} 0 & \Delta \\ \Delta & 0 \end{bmatrix}, \quad |\Psi(0)\rangle = |1\rangle \quad (76c)$$

$$\text{Model 4: } \hat{H}_Q = \begin{bmatrix} 0 & \Delta \\ \Delta & E \end{bmatrix}, \quad |\Psi(0)\rangle = |1\rangle \quad (76d)$$

$$\text{Model 5: } \hat{H}_Q = \begin{bmatrix} 0 & 0 & \Delta \\ 0 & E & 0 \\ \Delta & 0 & 0 \end{bmatrix}, \quad |\Psi(0)\rangle = |1\rangle \quad (76e)$$

$$\text{Model 6: } \hat{H}_Q = \begin{bmatrix} 0 & \Delta & \Delta \\ \Delta & E & 0 \\ \Delta & 0 & 0 \end{bmatrix}, \quad |\Psi(0)\rangle = |1\rangle \quad (76f)$$

$$\text{Model 7: } \hat{H}_Q = \begin{bmatrix} 0 & 0 & 0 \\ 0 & 0 & \Delta'' \\ 0 & \Delta'' & 0 \end{bmatrix}, \quad |\Psi(0)\rangle = |2\rangle \quad (76g)$$

$$\text{Model 8: } \hat{H}_Q = \begin{bmatrix} 0 & \Delta' & \Delta' \\ \Delta' & E' & 0 \\ \Delta' & 0 & 0 \end{bmatrix}, \quad |\Psi(0)\rangle = |1\rangle \quad (76h)$$

where $E = 3$ eV., $\Delta = 5$ eV., $E' = 1$ a.u., $\Delta' = 0.2$ a.u., and $\Delta'' = 3$ eV. The initial conditions $|\Psi(0)\rangle$ are also indicated accordingly. For Models 1-8, $\hat{H}_C + \hat{H}_{QC} = 0$, thus Eq. 12 is identical to Eq. 21, and the \mathcal{L} -MFE approach in Eq. 72 generates identical results as Eq. 21.

Molecule Coupled to a Lossy Cavity Mode. In addition, we consider a photo-isomerization model (without permanent dipole) coupled to a single optical cavity mode. The QED Hamiltonian for the molecule-cavity hybrid system is expressed as⁵⁸

$$\hat{H}_{\text{QED}} = \hat{H}_M + \hbar\omega_c \left(\hat{a}^\dagger \hat{a} + \frac{1}{2} \right) + \hbar g_c (\hat{a} + \hat{a}^\dagger) (\hat{\sigma}^\dagger + \hat{\sigma}). \quad (77)$$

In Eq. 77, \hat{H}_M is the molecular Hamiltonian described by a diabatic model system that undergoes an isomerization reaction⁵⁸

$$\hat{H}_M = \hat{T}_R + E_g(R)|g\rangle\langle g| + E_e(R)|e\rangle\langle e|. \quad (78)$$

Here, $|\alpha\rangle \in \{|g\rangle, |e\rangle\}$ represents the electronic ground or excited state, which are treated as diabatic states in this model, R represents the reaction coordinate, and $\hat{T}_R = \hat{P}^2/2M$ is the nuclear kinetic energy operator associated with R , with nuclear mass $M = 550$ Da. The detailed expression of $E_\alpha(R)$ is provided in Appendix C. The second term in Eq. 77 is the Hamiltonian of the quantized photon mode inside the cavity with the frequency ω_c , and \hat{a}^\dagger and \hat{a} are the photon creation and annihilation operators, respectively. The third term in Eq. 77 describes the molecule-photon coupling through electric-dipole interactions under the dipole gauge,⁵⁹ where $\hat{\sigma}^\dagger = |e\rangle\langle g|$ and $\hat{\sigma} = |g\rangle\langle e|$ are the molecular excitonic creation and

annihilation operators, respectively, and the light-matter interaction strength $\hbar g_c$ is treated as a parameter in this model.⁵⁸ The dipole self-energy $\frac{g_c^2}{\omega_c}$, which is a constant in this case due to the constant g_c , does not influence the quantum dynamics and is explicitly dropped in Eq. 77. This model can be viewed as the molecular version of the Quantum Rabi model.

A simplified version of the model in Eq. 77 can be constructed by dropping the counter-rotating wave terms proportional to $\hat{a}^\dagger \hat{\sigma}^\dagger$ and $\hat{a} \hat{\sigma}$. This approximation gives the Jaynes-Cummings model as

$$\hat{H}_{\text{JC}} = \hat{H}_M + \hbar\omega_c \left(\hat{a}^\dagger \hat{a} + \frac{1}{2} \right) + \hbar g_c (\hat{a} \hat{\sigma}^\dagger + \hat{a}^\dagger \hat{\sigma}). \quad (79)$$

We further denote the polariton Hamiltonian \hat{H}_{pl} as follows $\hat{H}_{\text{pl}} = \hat{H} - \hat{T}_R$. Representing the radiation field in its Fock state basis (the photon number state), and the molecule in its electronic state basis, the polariton Hamiltonian \hat{H}_{pl} (choosing $\hat{H} = \hat{H}_{\text{JC}}$) is expressed as

$$\begin{aligned} \hat{H}_{\text{pl}} = & \sum_{\alpha, n} \left(E_\alpha(R) + \left(n + \frac{1}{2} \right) \hbar\omega_c \right) |\alpha, n\rangle\langle\alpha, n| \quad (80) \\ & + \sum_{n=1}^{\infty} \sqrt{n} \hbar g_c (|e, n-1\rangle\langle g, n| + |g, n\rangle\langle e, n-1|), \end{aligned}$$

where $|\alpha, n\rangle = |\alpha\rangle \otimes |n\rangle$ is the electronic-photon basis (or exciton-Fock basis, composed of photon-dressed electronic states), with $|\alpha\rangle \in \{|g\rangle, |e\rangle\}$, and $|n\rangle$ is the Fock state of the radiation mode, *i.e.*, the eigenstate of $\hbar\omega_c (\hat{a}^\dagger \hat{a} + \frac{1}{2})$. The polariton states are the eigenstates of \hat{H}_{pl} , defined as $\hat{H}_{\text{pl}}|\Psi_p(R)\rangle = \mathcal{E}_p(R)|\Psi_p(R)\rangle$ where $\mathcal{E}_p(R)$ is the polariton potential and $|\Psi_p(R)\rangle$ is the polariton state.

The lifetime of the cavity mode is finite, due to the coupling between the cavity mode and the far-field photon modes outside the cavity. The detailed discussions for molecular cavity QED with cavity loss are provided in Appendix D. Here, we use the following Lindblad jump operator¹⁴ to model this process

$$\hat{L}_S = \hat{a} \otimes \hat{\mathcal{I}}_e \otimes \hat{\mathcal{I}}_R = \left[\sum_{n=1}^{\infty} \sqrt{n} |n-1\rangle\langle n| \right] \otimes \hat{\mathcal{I}}_e \otimes \hat{\mathcal{I}}_R, \quad (81)$$

where $\hat{\mathcal{I}}_e = |g\rangle\langle g| + |e\rangle\langle e|$ is the identity in the electronic subspace and $\hat{\mathcal{I}}_R$ is the identity operator in the nuclear subspace. The decay rate associated with \hat{L}_{cl} is denoted as Γ .

In this paper, we consider this photo-isomerization model under the Jaynes-Cummings approximation where there is a maximum of only one excitation (the single-excited subspace plus the ground state) because the light-matter coupling strength $\hbar g_c/\omega_c < 0.1$ thus the results do not significantly change when including states with multiple excitations. In this case, the possible Fock states are just $|n\rangle \in \{|0\rangle, |1\rangle\}$. Thus, the system Hamiltonian

\hat{H}_S can be written as

$$\begin{aligned} \hat{H}_S = & \hat{T}_R + E_g(R)|g, 0\rangle\langle g, 0| + E_e(R)|e, 0\rangle\langle e, 0| \quad (82) \\ & + (E_g(R) + \hbar\omega_c)|g, 1\rangle\langle g, 1| \\ & + \hbar g_c(|e, 0\rangle\langle g, 1| + |g, 1\rangle\langle e, 0|), \end{aligned}$$

and the system Lindblad jump operator can be written as

$$\hat{L}_S = |g, 0\rangle\langle g, 1| \otimes \hat{\mathcal{I}}_R, \quad (83)$$

with decay rate Γ which is varied as a parameter.

When using \mathcal{L} -MFE approach to simulate the dynamics of this molecule-cavity system, we consider the electronic and photonic DOFs as the quantum DOFs, where $\hat{H}_Q = \hbar\omega_c|g, 1\rangle\langle g, 1| + \hbar g_c(|e, 0\rangle\langle g, 1| + |g, 1\rangle\langle e, 0|)$, $\hat{H}_{QC} = E_g(R)(|g, 0\rangle\langle g, 0| + |g, 1\rangle\langle g, 1|) + E_e(R)|e, 0\rangle\langle e, 0|$, and the nuclear DOF is treated as a classical DOF, where $\hat{H}_C = \hat{T}_R$. The cavity frequency is $\omega_c = 1.632684$ e.V. and the coupling strength is $g_c = 0.136$ e.V. Note that the off-diagonal coupling terms in \hat{H}_S do not involve the ground state $|g, 0\rangle$; thus, the \mathcal{L} -MFE approach in Eq. 72 generates identical results as Eq. 21. The initial condition is $|\Psi(0)\rangle = |e, 0\rangle \otimes |\chi_0\rangle$, where the $|e, 0\rangle$ indicates the initial electronic-photonic state, and the nuclear wavefunction is $\langle R|\chi_0\rangle = \left(\frac{M\omega_R}{\pi}\right)^{1/4} e^{-(M\omega_R/2)(R-R_0)^2}$, which is a Gaussian wavepacket centered around $R_0 = -0.7$ a.u. with variance $1/2M\omega_R$, mass $M = 550$ Da, and frequency $\omega_R = 132.4$ cm^{-1} . The temperature is set to be $T = 0$ K. For the \mathcal{L} -MFE simulation, the corresponding initial condition is $\hat{\rho}_S(0) = |e, 0\rangle\langle e, 0| \otimes [\hat{\rho}_R]$, where the Wigner density of the nuclear wavefunction $[\hat{\rho}_R]_w = [|\chi_0\rangle\langle\chi_0|]_w = \frac{1}{\pi} e^{-M\omega_R(R-R_0)^2 - (P-P_0)^2/(M\omega_R)}$ is used to sample the initial nuclear position and momentum in the \mathcal{L} -MFE simulation.

Computational Details. The \mathcal{L} -MFE method is implemented by using a symmetrical Trotter decomposition in Eq. 72 to reduce time step error. The unitary dynamics $e^{-\frac{i}{\hbar}(\hat{H}_Q + \hat{H}_{QC})dt}$ are propagated using the 4th order Runge Kutta (RK4) algorithm, while the Lindblad decay dynamics $\hat{\mathcal{T}}$ are propagated using the coefficient modifications described in Eqs. 69a to 71. When classical nuclear DOFs are present, the velocity Verlet algorithm is used to propagate the nuclear DOFs, with mean-field force given by Eq. 16, alongside the quantum subsystem. For all model calculations, the electronic time step used is $dt_E = 0.05$ a.u. For the photo-isomerization system that contains nuclear DOF, the nuclear time step was $dt_N = 6$ a.u. and the time step used in the Lindblad decay $\hat{\mathcal{T}}$ was $dt_N/4$ (thus the unitary propagation was performed 60 times in between Lindblad decay propagations). A total of 24,000 trajectories were used to ensure fully converged results, although using only 1000 trajectories already provides a mostly converged result (as shown in Fig. 3).

The numerical results obtained from \mathcal{L} -MFE were benchmarked against the original Lindblad dynamics in

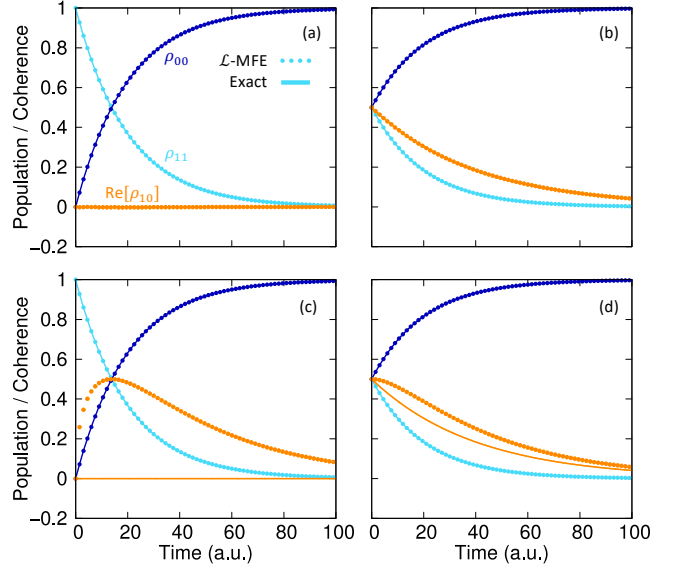


FIG. 1. Dynamics of (a) Model 1 and (b) Model 2. The solid lines are exact Lindblad dynamics while the dotted lines are the \mathcal{L} -MFE method. The cyan lines are the population of state $|1\rangle$, the dark blue lines are the population of state $|0\rangle$, and the orange lines represent $\text{Re}[\rho_{10}]$. Panels (c)-(d) present the same calculation as (a) and (b), but without any random phase (by setting $\theta_\xi = 0$ in Eq. 69b) in the \mathcal{L} -MFE method, thus generating artificially large coherence.

Eq. 21, which are referred to as “exact” results (of performing Lindblad dynamics) in this paper. These numerical results are obtained by using the QuTiP library^{60,61} with the mesolve function, where model Hamiltonian, Lindblad jump operator, and initial wavefunction are entered as arguments to the function. Similar numerical simulations has been recently performed to investigate molecular cavity QED processes as well.^{14–16} For Models 1-8, $\hat{H}_C + \hat{H}_{QC} = 0$ (no nuclear DOF), and the only inputs in the simulation are the matrix elements of \hat{H}_Q and the decay rate Γ . For the photo-isomerization coupled to the cavity model, \hat{H}_S is described by Eq. 82. The matrix elements of the Hamiltonian in Eq. 82 as well as the jump operator \hat{L}_S in Eq. 83 are evaluated using the basis $\{|\alpha, n\rangle \otimes |\chi_\nu\rangle\}$, where $|\chi_\nu\rangle$ is the discrete variable representation (DVR) basis for the nuclear DOF R . For the DVR basis $|\chi_\nu\rangle$, a total of 175 grid points are used in the range of $R \in [-1.25$ a.u., 1.25 a.u.].

V. RESULTS AND DISCUSSION

Fig. 1a presents the population dynamics of Model 1 (Eq. 76a), obtained from the \mathcal{L} -MFE approach (dots) as well as exact Lindblad dynamics (solid lines). In this case, the only dynamics present are the Lindblad exponential decay from state $|1\rangle$ to state $|0\rangle$. In Fig. 1a, the diagonal populations of both states $|1\rangle$ and $|0\rangle$ exhibit the expected exponential decay/growth at a rate of $\Gamma = 0.05$,

while the coherence between the two states stays at 0. This is expected because, in the absence of any Hamiltonian dynamics, the coherences between states $|1\rangle$ and $|0\rangle$ should only monotonically decrease to 0 from the initial time coherence $\rho_{01}(0)$. Fig. 1b presents the population dynamics of Model 2 (Eq. 76b), which has an initial condition of a superposition of state $|1\rangle$ and $|0\rangle$. Similar to Model 1, only Lindblad exponential decay/growth is present. The diagonal populations match the Lindblad dynamics, and the coherence shows the expected $\Gamma/2$ decay rate from Lindblad dynamics.

We note that because $\hat{H}_Q = 0$ in Models 1 & 2, the \mathcal{L} -MFE method in Eq. 72 becomes $\mathbf{c}(t + dt) = \hat{\mathcal{T}}(dt) \cdot \mathbf{c}(t)$, where the dynamics are completely dictated by the Lindblad decay process governed by $\mathcal{L}_{\hat{L}}$. The dynamics are insensitive to the choice of dt , which means that one can choose an arbitrarily large dt and obtain identical results. This is not the case for Ehrenfest+R approach, where the “+R” dynamics will be sensitive to the choice of dt even when $\hat{H}_Q = 0$.

Fig. 1c-d present the incorrect dynamics when the random phases θ_ξ (in Eq. 69b) are intentionally ignored by setting them to be zero. One can see that the diagonal populations of states $|1\rangle$ and $|0\rangle$ still show the correct exponential decay/growth, but the coherences take a large departure from the expected coherences because there is no random phase present to correct the artificial coherence that is produced when the magnitudes of the coefficients are changed.

Fig. 2a presents the population dynamics of Model 3 (Eq. 76c). This model contains Hamiltonian-induced coherences (through the Δ term in Eq. 76c) which must be properly incorporated with the Lindblad decay dynamics. In Fig. 2a, the diagonal populations match the exact Lindblad dynamics result with both correct oscillation magnitudes and correct longtime populations. The oscillations of the imaginary parts (dark and light orange lines) of the off-diagonal coherences also exactly agree with Lindblad dynamics. Fig. 2b presents the population dynamics of Model 4 (Eq. 76d), which contains both electronic coupling as well as an energy level difference between the two states, which will further impact the dynamics. Again, both the diagonal populations and the off-diagonal coherences match the exact Lindblad dynamics.

Fig. 2c-d present the incorrect dynamics when the random phases θ_ξ (in Eq. 69b) are intentionally ignored by setting them to be zero. In Fig. 2c, the longtime diagonal populations appear correct, but the diagonal populations oscillate with a much larger magnitude than Lindblad dynamics. This is caused by the fact that the coherences are larger than they should be because there is no random phase to reduce the size of the coherences. Consequentially, the larger magnitude of coherence causes a larger magnitude of population oscillations. In Fig. 2d, not only are the oscillation magnitudes of the diagonal populations too large, but the diagonal populations converge to incorrect longtime populations. In fact, the \mathcal{L} -MFE

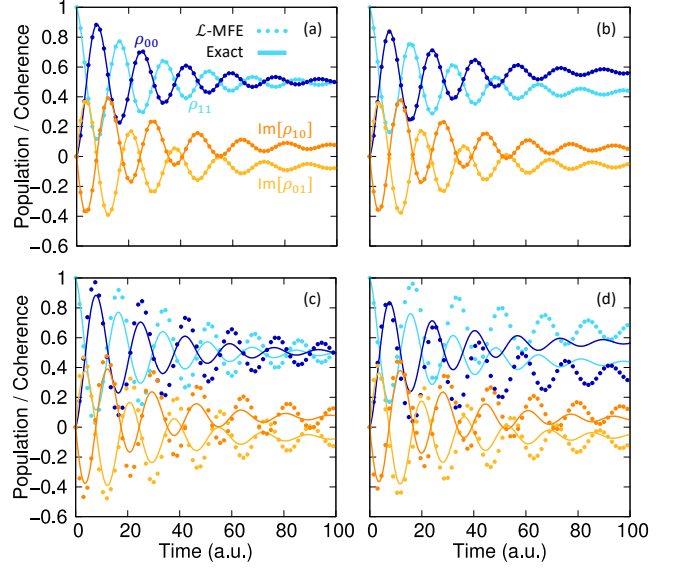


FIG. 2. Dynamics of (a) Model 3 and (b) Model 4. The solid lines are exact Lindblad dynamics while the dotted lines are the \mathcal{L} -MFE method. The cyan lines are the population of state $|1\rangle$, the dark blue lines are the population of state $|0\rangle$, the darker orange lines represent $\text{Im}[\rho_{10}]$, and the lighter orange lines represent $\text{Im}[\rho_{01}]$. Panels (c)-(d) present the same calculation as (a) and (b), but without any random phase (by setting $\theta_\xi = 0$ in Eq. 69b) in the \mathcal{L} -MFE method.

method with no random phase shows the excited state $|1\rangle$ with a larger longtime population, while Lindblad dynamics show that the ground state $|0\rangle$ should have the larger longtime population. This is again caused by the incorrect coherences without random phase which cause a longtime shift in the diagonal populations.

Fig. 3 presents the population dynamics of Model 4 (Eq. 76d) with different numbers of trajectories to examine the convergence of the \mathcal{L} -MFE method. The numbers of trajectories used in Fig. 3a-d are (a) 10, (b) 100, (c) 1,000, and (d) 10,000, respectively. For the result using 10 trajectories, the magnitudes and phases of the oscillations of the \mathcal{L} -MFE dynamics do not match the exact ones. However, the longtime populations of the states are approximately correct, in contrast to the no-random-phase case in Fig. 2d where the relative magnitude of the longtime populations are flipped versus the exact populations. For the result using 100 trajectories, the magnitudes of the oscillations are almost correct while there are some deviations at later times. For 1,000 trajectories, the relative error of the \mathcal{L} -MFE dynamics versus the exact dynamics is only a few percent, and there is little visual difference between the \mathcal{L} -MFE dynamics and the exact Lindblad dynamics. For 10,000 trajectories, the \mathcal{L} -MFE dynamics and exact Lindblad dynamics are nearly indistinguishable. These results give a better sense of how many trajectories are required to achieve a desired level of accuracy using the \mathcal{L} -MFE method.

Fig. 4a presents the population dynamics of Model

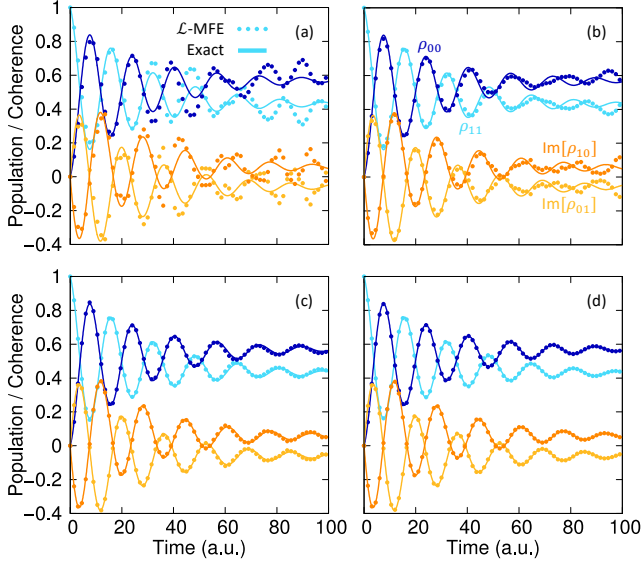


FIG. 3. Dynamics of Model 4 with different numbers of trajectories. The solid lines are exact Lindblad dynamics while the dotted lines are the \mathcal{L} -MFE method. The numbers of trajectories used are (a) 10, (b) 100, (c) 1,000, and (d) 10,000.

5 (Eq. 76e). This model contains the third state $|2\rangle$, which is coupled to state $|0\rangle$. Note that in the \mathcal{L} -MFE algorithm, when the jump operator is $\hat{L} = |0\rangle\langle 1|$, state $|0\rangle$ is the state that gains random phases (see Eq. 65). Thus, the preservation of correct dynamics when random phases interact with states $\{|j\rangle\}$ outside of the reduced density matrix of $|0\rangle$ and $|1\rangle$ is tested. In Fig. 4a, the excited state shows exponential decay, while states $|0\rangle$ and $|2\rangle$ oscillate together until they reach a longtime population of 0.5, which is predicted by Lindblad dynamics. In Fig. 4c, the corresponding imaginary parts of coherences $\text{Im}[\rho_{10}]$ (orange), $\text{Im}[\rho_{12}]$ (green), and $\text{Im}[\rho_{20}]$ (red) are presented, and all of these coherences obtained from \mathcal{L} -MFE (dotted) match the Lindblad dynamics (solid lines). In particular, the oscillation in $\text{Im}[\rho_{20}]$ is due to the presence of electronic coupling between state $|0\rangle$ and $|2\rangle$, without further decoherence from \hat{L} (see Eq. 24), suggesting that the \mathcal{L} -MFE method can correctly describe dynamics involving $\{|j\rangle\}$ states even in the presence of random phases in the coefficient of state $|0\rangle$.

Fig. 4b presents the population dynamics of Model 6 (Eq. 76f), which is a more challenging 3-state Hamiltonian that involves multiple electronic couplings to test the validity of the \mathcal{L} -MFE method. The diagonal populations generated from \mathcal{L} -MFE (dotted) again match Lindblad dynamics (solid lines). In Fig. 4d, all of the coherences, $\text{Im}[\rho_{10}]$ (orange), $\text{Im}[\rho_{12}]$ (yellow), and $\text{Im}[\rho_{20}]$ (red) match perfectly with Lindblad dynamics. Note that due to the electronic couplings between states $|0\rangle$ and $|1\rangle$, as well as between states $|0\rangle$ and $|2\rangle$, all of the coherences in general will be non-zero at a given point in time. Using the random phase (governed by Eq. 66)

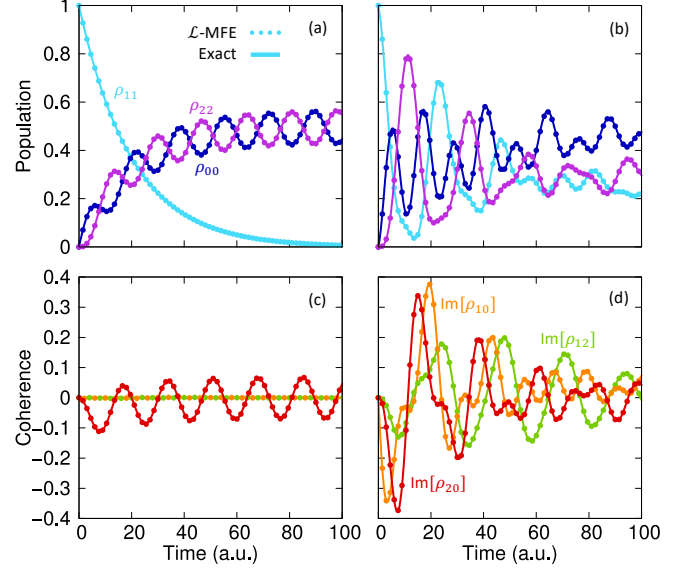


FIG. 4. Dynamics of Models 5 (a,c) and Model 6 (b,d). The solid lines are exact Lindblad dynamics while the dotted lines are the \mathcal{L} -MFE method. Panels (a) and (b) present the diagonal populations, with $\rho_{00}(t)$ (dark blue), $\rho_{11}(t)$ (cyan), and $\rho_{22}(t)$ (magenta). Panels (c) and (d) present the off-diagonal coherences, with $\text{Im}[\rho_{10}](t)$ (orange), $\text{Im}[\rho_{12}](t)$ (green), and $\text{Im}[\rho_{20}](t)$ (red).

for state $|0\rangle$, all of these detailed features are captured, further demonstrating the exact equivalence between the \mathcal{L} -MFE method and Lindblad dynamics when no nuclear DOFs are present.

Fig. 5 presents the population dynamics of Model 7 (Eq. 76g) to assess the importance of which state the random phase is applied to. Fig. 5a,c present the population and coherence dynamics, respectively, of the \mathcal{L} -MFE method versus exact Lindblad dynamics. The \mathcal{L} -MFE method applies the random phase only to state $|0\rangle$ and its dynamics match the exact results. Fig. 5b,d present the incorrect population and coherence dynamics, respectively, of a modified \mathcal{L} -MFE method when the random phase (θ_ξ) is only applied to state $|1\rangle$ instead of state $|0\rangle$, such that $c_{1,\xi}(t+dt) = e^{i\theta_\xi} e^{-\Gamma dt/2} c_{1,\xi}(t)$. The populations dynamics of this modified \mathcal{L} -MFE method show incorrect oscillation magnitudes, most notably that the oscillations between states $|1\rangle$ and $|2\rangle$ are considerably smaller than the oscillations of the exact dynamics. This corresponds to the coherence dynamics of $\text{Im}[\rho_{12}]$ that are smaller than the corresponding exact coherence dynamics. This coherence inaccuracy is caused by the over-decoherence of state $|1\rangle$ due to the application of the random phase to state $|1\rangle$. This result highlights the importance of applying the random phase to the correct state.

Fig. 6 presents the comparison, using Model 8 (Eq. 76h), between the original Ehrenfest+R approach^{10,11} and a modified Ehrenfest+R approach using the modified γ_R from Eq. 75 (which is equivalent to the \mathcal{L} -MFE

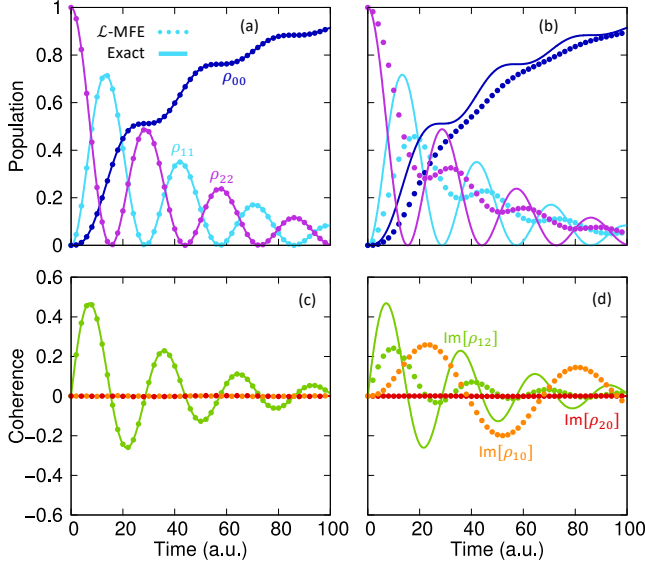


FIG. 5. Dynamics of Model 7 using (a,c) the \mathcal{L} -MFE approach and (b,d) a modified \mathcal{L} -MFE approach with the random phase only applied to state $|1\rangle$. The solid lines are exact Lindblad dynamics while the dotted lines are the original or modified \mathcal{L} -MFE approach. Panels (a) and (b) present the diagonal populations, with $\rho_{00}(t)$ (dark blue), $\rho_{11}(t)$ (cyan), and $\rho_{22}(t)$ (magenta). Panels (c) and (d) present the off-diagonal coherences, with $\text{Im}[\rho_{10}](t)$ (orange), $\text{Im}[\rho_{12}](t)$ (green), and $\text{Im}[\rho_{20}](t)$ (red).

method for this model). Fig. 6a,c present the population and coherence dynamics, respectively, obtained from Ehrenfest+R (dots), using the same algorithm as described in Ref. 11, where a concise summary of this approach can be found in Appendix A. The +R decay dynamics are implemented as suggested as the original reference¹⁰ (through Eq. A27a and Eq. A27b) using the original γ_R (Eq. A22b). The parameters of Model 8 were carefully chosen such that the excited state energy $E' = 1$ a.u. is significantly larger than the decay rate $\Gamma = 0.05$ a.u., such that the Ehrenfest+R method should work correctly in the regime $E' \gg \Gamma$, while still showing interesting dynamics on the timescale of the population decay ($t = 0 \sim 100$ a.u.). In Fig. 6a, the Ehrenfest+R dynamics are qualitatively similar to the exact Lindblad dynamics, but there are some errors in the fluctuations of the state $|1\rangle$ decay as well as in the magnitudes of the oscillations of states $|0\rangle$ and $|2\rangle$. The cause of these deviations can be seen in Fig. 6c, where the magnitudes of the coherences obtained from Ehrenfest+R are larger than those of Lindblad dynamics, causing incorrect population transfer between diagonal populations. This is because the coherence decay rate γ_R (Eq. A22b) in the Ehrenfest+R algorithm is smaller than the correct decay rate γ'_R (Eq. B11), causing artificially large coherences and thus a larger magnitude of population oscillation.

Fig. 6b,d present the population and coherence dynamics, respectively, of Model 8 (Eq. 76h) using the modified

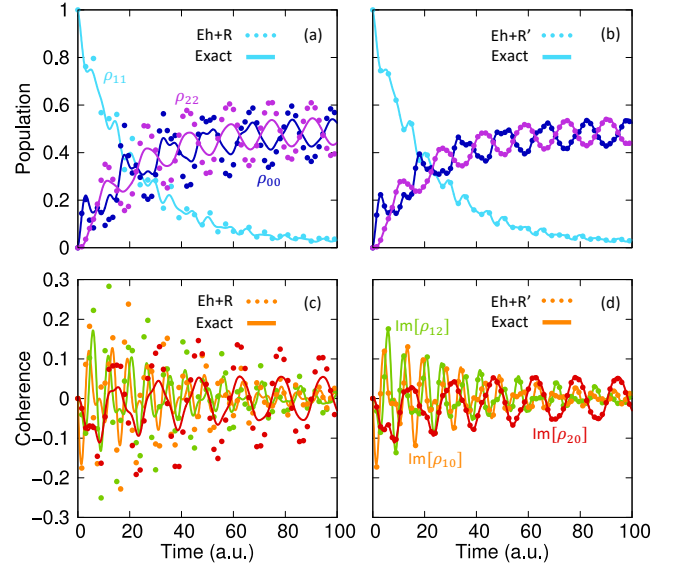


FIG. 6. Dynamics of Model 8 using (a,c) the original Ehrenfest+R approach (labeled as Eh+R) and (b,d) the Ehrenfest+R approach using the modified γ'_R from Eq. 75 (labeled as Eh+R'). The modified Ehrenfest+R dynamics (Eh+R') are identical to those obtained from the \mathcal{L} -MFE method for this model. The solid lines are exact Lindblad dynamics while the dotted lines are the original or modified Ehrenfest+R approach. Panels (a) and (b) present the diagonal populations, with $\rho_{00}(t)$ (dark blue), $\rho_{11}(t)$ (cyan), and $\rho_{22}(t)$ (magenta). Panels (c) and (d) present the off-diagonal coherences, with $\text{Im}[\rho_{10}](t)$ (orange), $\text{Im}[\rho_{12}](t)$ (yellow), and $\text{Im}[\rho_{20}](t)$ (red).

Ehrenfest+R approach that uses the modified γ'_R . This modified Ehrenfest+R approach produces results identical to those obtained from the \mathcal{L} -MFE method for this model. Consequentially, in Fig. 6b, the population dynamics of the modified Ehrenfest+R approach are identical to the Lindblad population dynamics. The corresponding coherence dynamics are provided in Fig. 6d, which again match perfectly with the Lindblad coherence dynamics. This demonstrates that it is important to include the effect that modifying the magnitudes of the coefficients has on the coherences between the states (see analysis in Appendix B). We note that using the modified γ'_R in the Ehrenfest+R method yields the same expectation values for the populations and coherences as the \mathcal{L} -MFE method as $\Gamma dt \rightarrow 0$, but begins to lose accuracy for larger Γdt due to the use of a Poisson process for decoherence (through Eq. A28), which is sensitive to the choice of Γdt (Eq. B7).

Fig. 7 presents the potential energy surfaces (PESs) and population dynamics of the photo-isomerization model coupled to an optical cavity, with the system Hamiltonian described in Eq. 82. Here, we explicitly consider the population decay of the photonic DOF through the jump operator \hat{L} in Eq. 83, which describes the finite lifetime of the cavity mode due to its coupling to the other non-cavity modes.

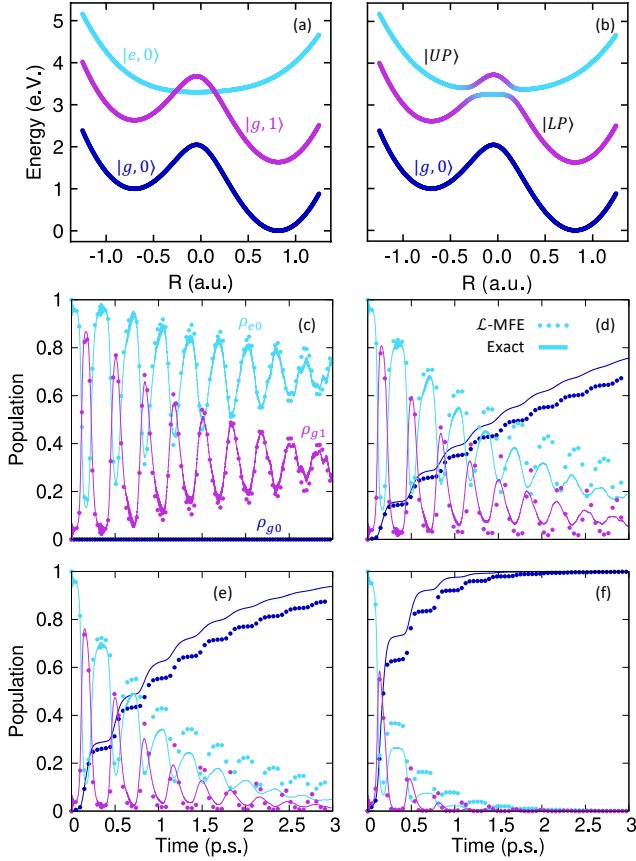


FIG. 7. Potential energy surfaces (PESs) and population dynamics of the model isomerization reaction coupled to the cavity. Panel (a) presents the diabatic PESs where the dark blue line is the $|g,0\rangle$ PES, the cyan line is the $|e,0\rangle$ PES, and the magenta line is the $|g,1\rangle$ PES. Panel (b) presents the adiabatic PESs where the dark blue line is the ground state $|g,0\rangle$ PES, the middle line (labeled $|LP\rangle$) is the lower polariton PES, and the upper line (labeled $|UP\rangle$) is the upper polariton PES. The colors along the adiabatic PESs represent the diabatic character at each nuclear position. Panels (c)-(f) present the population dynamics where (c) uses a decay rate of $\Gamma = 0$, (d) uses $\Gamma = 1$ meV, (e) uses $\Gamma = 2$ meV, and (f) uses $\Gamma = 8$ meV. The solid lines are exact Lindblad dynamics while the dotted lines are the \mathcal{L} -MFE method. The dark blue lines are the state $|g,0\rangle$ populations, the cyan lines are the state $|e,0\rangle$ populations, and the magenta lines are the state $|g,1\rangle$ populations.

Fig. 7a presents the diabatic PESs for the $|g,0\rangle$ state (dark blue), the $|e,0\rangle$ state (cyan), and the $|g,1\rangle$ state (magenta). These states are diabatic because their electronic character does not depend on the nuclear coordinate R , thus there is no derivative coupling between these states (see Appendix C for details). Conversely, there is a diabatic coupling between the states $|e,0\rangle$ and $|g,1\rangle$ which causes coherent population transfer between these states. Fig. 7b presents the adiabatic PESs for the ground $|g,0\rangle$ state (dark blue), the lower polariton state (middle line, labeled $|LP\rangle$), and the upper polariton

state (upper line, labeled $|UP\rangle$). These adiabatic states are eigenstates of the polaritonic Hamiltonian $\hat{H}_S - \hat{T}_R$ (where \hat{H}_S is given in Eq. 82) thus there is no additional diabatic coupling between any of the states. Further, since the electronic character of the upper and lower polariton states changes as a function of the nuclear coordinate R , there exists derivative coupling between the upper and lower polariton states which allows for coherent population transfer between them.⁶²

Fig. 7c-f presents the population dynamics of diabatic states $|g,0\rangle$ (dark blue), $|e,0\rangle$ (cyan), and $|g,1\rangle$ (magenta). The results of exact Lindblad dynamics (solid lines) are obtained by solving Eq. 12 using the basis $\{|\alpha, n\rangle \otimes |\chi_\nu\rangle\}$, where $|\alpha, n\rangle = |\alpha\rangle \otimes |n\rangle$, $|\alpha\rangle \in \{|g\rangle, |e\rangle\}$ are the diabatic electronic states and $|n\rangle$ are the Fock states of the cavity mode. The \mathcal{L} -MFE dynamics (dotted) are obtained by treating the electronic and photonic DOFs as the quantum subsystem, with basis $|\alpha, n\rangle$, and the nuclear DOF as a classical DOF. The details of these numerical simulations are provided in Sec. IV.

Fig. 7c presents the population dynamics with $\Gamma = 0$, *i.e.*, with no Lindblad decay dynamics. Thus, Eq. 12 reduces to the exact dynamics of a closed system with the Hamiltonian in Eq. 82 (which is a molecule-cavity hybrid system), and Eq. 21 reduces to the Ehrenfest dynamics for the same system. The Ehrenfest dynamics provides nearly identical results compared to the exact dynamics in this case because the nuclei are mostly oscillating on a single adiabatic upper polariton surface (see Fig. 7b). Because there are no interactions between the $|g,0\rangle$ state and the other states in the model, the $|g,0\rangle$ state is not populated.

In Fig. 7d, the Lindblad jump operator interaction strength is set to be $\Gamma = 1$ meV, which causes the population of the upper and lower polariton states to decay to the ground state $|g,0\rangle$ of the molecule cavity hybrid system. While the \mathcal{L} -MFE dynamics semi-quantitatively match the exact Lindblad dynamics, there are some noticeable differences in the magnitudes of oscillation of states $|e,0\rangle$ and $|g,1\rangle$, and the ground state $|g,0\rangle$ does not rise as quickly as predicted by Lindblad dynamics. Similarly, in Fig. 7e-f, when the interaction strength is set to be $\Gamma = 2$ meV and $\Gamma = 8$ meV, respectively, the \mathcal{L} -MFE dynamics show similar errors while still maintaining the semi-quantitatively correct dynamics.

The discrepancy between the dynamics obtained from the \mathcal{L} -MFE method and the exact Lindblad dynamics is due to the inadequacy of MFE as a mixed quantum-classical method. This demonstrates the need to incorporate Lindblad dynamics into more accurate mixed quantum-classical or semiclassical approaches that go beyond the approximations present in the mean-field Ehrenfest approach. Note that in recent investigations of molecular cavity quantum electrodynamics,^{28,63} the photonic population decay is incorporated in a similar fashion as described in Eq. 69a-69c. However, in these early investigations, the random phase $e^{i\theta_\epsilon}$ (in Eq. 69b) is not incorporated. We have demonstrated the consequence of

missing this random phase in Fig. 1-2, where artificial coherences are generated. Future wavefunction based investigations in molecular cavity QED should carefully describe the decay dynamics using the approach outlined in \mathcal{L} -MFE.

VI. CONCLUSIONS

In this work, we derived the \mathcal{L} -MFE method to incorporate Lindblad jump operator dynamics into the mean-field Ehrenfest (MFE) approach. We took the density matrix equations of motion for Lindblad dynamics and mapped them onto an ensemble of pure state coefficients, using trajectory averages and expectation values of random variables. We then derived the \mathcal{L} -MFE method to update the MFE coefficients at each time step which rigorously satisfies Lindblad jump operator dynamics. This established a method that exactly reproduces Lindblad decay dynamics using a wavefunction description, with deterministic changes of the magnitudes of the quantum expansion coefficients, while only adding on a stochastic phase (on coefficients $c_{0,\xi}(t)$ in Eq. 69b).

Compared to the Monte Carlo wavefunction methods^{35,36} which randomly collapse the wavefunction onto single states, the \mathcal{L} -MFE approach only adds on random phases to the expansion coefficients, providing a more stable dynamics which can be incorporated with any mixed quantum-classical, semiclassical, or wavepacket based approaches. Compared to the Ehrenfest+R method^{10,11} the \mathcal{L} -MFE method uses the same procedure to decay the magnitude of the quantum expansion coefficients, but a different choice of the random phase distribution, such that the exact Lindblad dynamics can be recovered, whereas Ehrenfest+R cannot exactly recover Lindblad dynamics. The derivation procedure of \mathcal{L} -MFE also does not assume any relation between the energy gap of the two states versus the decay rate, whereas Ehrenfest+R assumes a particular parameter regime where the energy gap is much larger than the decay rate. Our theoretical analysis further provides valuable insights and mathematical justification for the relationship between the dynamics of the reduced density matrix and the dynamics of the ensemble of pure states. Through these careful analyses, we discovered an easy fix of the Ehrenfest+R method with the correct “+R” decay rate, which can be used to fix Ehrenfest+R dynamics to exactly reproduce Lindblad dynamics.^{10,11}

Throughout the theoretical development in this work, we demonstrated the importance of including a carefully chosen random phase on both the coherences as well as the diagonal populations of the dynamics. Using numerical simulations, we demonstrated that the \mathcal{L} -MFE method is equivalent to Lindblad dynamics for a variety of complicated dynamical scenarios when nuclear DOFs are not present, including scenarios where previous approaches (such as Ehrenfest+R^{10,11}) do not match Lindblad dynamics. We further demonstrated

that when including nuclei in Ehrenfest dynamics, the \mathcal{L} -MFE method gives semi-quantitatively accurate results, with the accuracy limited by the accuracy of the approximations present in the semiclassical MFE approach.

This work provides a general approach for incorporating the Markovian dynamics of the Lindblad master equation into a scalable, wavefunction-type approach, allowing for the description of the dynamics of a quantum subsystem interacting with an anharmonic classical subsystem (nuclei) through a mixed quantum-classical description, as well as a Markovian environment that can be accurately described by Lindblad dynamics. The current approach can readily be used in the context of describing spontaneous emission due to light-matter interactions,^{10,35} incorporating cavity leaking in polariton chemistry,^{14–16,28,63} or being combined with Ehrenfest dynamics^{18,19,38,64} or a surface hopping approach⁴ to incorporate decoherence corrections. We envision that the current approach provides a general framework for future work to incorporate Lindblad dynamics into other mixed quantum-classical or semiclassical approaches.

ACKNOWLEDGMENTS

This work was supported by the National Science Foundation “Center for Quantum Electrodynamics for Selective Transformations (QuEST)” under the Grant number CHE-2124398. E.R.K. and A.M. are partially supported by the University Research Award from the University of Rochester. Computing resources were provided by the Center for Integrated Research Computing (CIRC) at the University of Rochester.

CONFLICT OF INTEREST

The authors have no conflicts to disclose.

AVAILABILITY OF DATA

The data that support the findings of this study are available from the corresponding author upon a reasonable request.

Appendix A: The Ehrenfest+R Approach

The Ehrenfest+R method¹⁰ was originally developed to simulate the electronic quantum subsystem during a spontaneous emission process while accurately describing the feedback of the quantum dynamics onto the classical electromagnetic field. While the Lindblad master equation was not used to derive the equations of motion for the quantum subsystem during spontaneous emission,

the resulting equations of motion for the quantum subsystem are mathematically identical to those of the Lindblad master equation for a two level uncoupled system with a decay from an excited state to a ground state. Thus, while the Ehrenfest+R method was not originally intended to broadly describe and simulate Lindblad dynamics for generic quantum subsystems, the method should be, in principle, able to do exactly this (at least when the energy gap is much larger than the decay rate). Additionally, Ehrenfest+R was a primary source of inspiration for the \mathcal{L} -MFE method derived in this paper, so it is fruitful to examine the quantum subsystem part of the Ehrenfest+R method in order to understand its relation to the \mathcal{L} -MFE method and to understand any potential issues it has.

The Ehrenfest+R method may generally be applied to the spontaneous emission between any two quantum states as long as the energy gap is much larger than the decay rate. For simplicity, a two-level system will be considered to clearly understand the method, as was done in the original paper¹⁰. Consider a two-level system with the following quantum subsystem Hamiltonian \hat{H}_Q and a Lindblad jump-operator \hat{L} defined as follows

$$\hat{H}_Q = \begin{bmatrix} 0 & 0 \\ 0 & E \end{bmatrix}, \quad \hat{L} = |0\rangle\langle 1|, \quad (\text{A1})$$

where the jump operator has a decay rate $\Gamma \ll E$. Throughout the discussion of the Ehrenfest+R approach, we ignore the presence of $\hat{H}_{QC}(\mathbf{R}) + \hat{H}_C$ (see Eq. 5), although it is possible to generalize it to incorporate these terms. The Lindblad decay superoperator $\mathcal{L}_{\hat{L}}$ (whose effect is given in Eq. 25) corresponding to the decay dynamics can be written in the *Liouville space* as follows

$$\mathcal{L}_{\hat{L}} = \begin{bmatrix} 0 & 0 & 0 & \Gamma \\ 0 & -\Gamma/2 & 0 & 0 \\ 0 & 0 & -\Gamma/2 & 0 \\ 0 & 0 & 0 & -\Gamma \end{bmatrix}, \quad (\text{A2})$$

where its effect on the reduced density matrix elements $\rho_{ab} = \langle \psi_a | \hat{\rho}(t) | \psi_b \rangle$ (in the Liouville space) is expressed as

$$\mathcal{L}_{\hat{L}}[\hat{\rho}(t)] = \mathcal{L}_{\hat{L}} \begin{bmatrix} \rho_{00} \\ \rho_{01} \\ \rho_{10} \\ \rho_{11} \end{bmatrix} = \begin{bmatrix} \Gamma\rho_{11} \\ -\frac{\Gamma}{2}\rho_{01} \\ -\frac{\Gamma}{2}\rho_{10} \\ -\Gamma\rho_{11} \end{bmatrix}. \quad (\text{A3})$$

The overall time evolution of $\hat{\rho}$, governed by Eq. 21, is

$$\frac{d\hat{\rho}}{dt} = \mathcal{L}_{\hat{H}}[\hat{\rho}] + \mathcal{L}_{\hat{L}}[\hat{\rho}] \equiv \mathcal{L}[\hat{\rho}], \quad (\text{A4})$$

where the total Lindblad Liouvillian superoperator $\mathcal{L} = \mathcal{L}_{\hat{H}} + \mathcal{L}_{\hat{L}}$ in the Liouville space is expressed as

$$\mathcal{L} = \begin{bmatrix} 0 & 0 & 0 & \Gamma \\ 0 & iE - \frac{\Gamma}{2} & 0 & 0 \\ 0 & 0 & -iE - \frac{\Gamma}{2} & 0 \\ 0 & 0 & 0 & -\Gamma \end{bmatrix}, \quad (\text{A5})$$

which is $\mathcal{L}_{\hat{L}}$ (Eq. A2) plus $\mathcal{L}_{\hat{H}}$ in the Liouville space.

The effect of this Liouvillian on the reduced density matrix elements, written in the Liouville space, is

$$\mathcal{L}[\hat{\rho}(t)] = \mathcal{L} \begin{bmatrix} \rho_{00} \\ \rho_{01} \\ \rho_{10} \\ \rho_{11} \end{bmatrix} = \begin{bmatrix} \Gamma\rho_{11} \\ (iE - \frac{\Gamma}{2})\rho_{01} \\ (-iE - \frac{\Gamma}{2})\rho_{10} \\ -\Gamma\rho_{11} \end{bmatrix}. \quad (\text{A6})$$

The Liouvillian in Eq. A5 can be matrix-exponentiated to determine the propagator of the density matrix during a time step dt as

$$e^{\mathcal{L}dt} = \begin{bmatrix} 1 & 0 & 0 & 1 - e^{-\Gamma dt} \\ 0 & e^{iE dt - \Gamma dt/2} & 0 & 0 \\ 0 & 0 & e^{-iE dt - \Gamma dt/2} & 0 \\ 0 & 0 & 0 & e^{-\Gamma dt} \end{bmatrix}, \quad (\text{A7})$$

where the above propagator $e^{\mathcal{L}dt}$ evolves the reduced density operator as

$$e^{\mathcal{L}dt}[\hat{\rho}(t)] = \begin{bmatrix} \rho_{00} + \rho_{11}(1 - e^{-\Gamma dt}) \\ \rho_{01}e^{iE dt - \Gamma dt/2} \\ \rho_{10}e^{-iE dt - \Gamma dt/2} \\ \rho_{11}e^{-\Gamma dt} \end{bmatrix}. \quad (\text{A8})$$

While the dynamics described by the Lindblad Liouvillian in Eq. A5 are identical to the quantum subsystem dynamics that the Ehrenfest+R method aims to simulate, the particular implementation of the method was developed by additionally considering the role the electromagnetic field should have in spontaneous emission. The authors Chen et al. derive a Hamiltonian interaction term (not present in Eq. A1) that represents the electric dipole coupling between the excited and ground states of the system. This time-dependent interaction term \hat{H}_{int} is defined as follows

$$\hat{H}_{\text{int}} = \Omega \cdot (|0\rangle\langle 1| + |1\rangle\langle 0|) = -\hbar\Gamma \cdot \text{Im}[\rho_{01}] (|0\rangle\langle 1| + |1\rangle\langle 0|). \quad (\text{A9})$$

This extra interaction term is added to the original \hat{H}_Q which defines the effective Ehrenfest Hamiltonian \hat{H}_{Eh} as follows

$$\hat{H}_{\text{Eh}} = \hat{H}_Q + \hat{H}_{\text{int}} = \begin{bmatrix} 0 & \Omega \\ \Omega & E \end{bmatrix}, \quad (\text{A10})$$

with $\Omega = -\hbar\Gamma \cdot \text{Im}[\rho_{01}]$. The Hamiltonian in Eq. A10 is the Hamiltonian that is used to propagate the dynamics during the first stage of the Ehrenfest+R method (the ‘‘Ehrenfest’’ stage). The time evolution of $\hat{\rho}$ governed by \hat{H}_{Eh} is thus

$$\frac{d\hat{\rho}}{dt} = -\frac{i}{\hbar} [\hat{H}_{\text{Eh}}, \hat{\rho}] = \mathcal{L}_{\text{Eh}}[\hat{\rho}], \quad (\text{A11})$$

where the Liouvillian \mathcal{L}_{Eh} is expressed as

$$\mathcal{L}_{\text{Eh}} = \begin{bmatrix} 0 & i\Omega & -i\Omega & 0 \\ i\Omega & iE & 0 & -i\Omega \\ -i\Omega & 0 & -iE & i\Omega \\ 0 & -i\Omega & i\Omega & 0 \end{bmatrix}, \quad (\text{A12})$$

and the time evolution rate of $\hat{\rho}$ governed by \mathcal{L}_{Eh} in the Liouville space is expressed as

$$\mathcal{L}_{\text{Eh}}[\hat{\rho}(t)] = \begin{bmatrix} 2\Gamma \cdot \text{Im}[\rho_{01}]^2 \\ iE\rho_{01} + i\Gamma \cdot \text{Im}[\rho_{01}](\rho_{11} - \rho_{00}) \\ -iE\rho_{10} - i\Gamma \text{Im}[\rho_{01}](\rho_{11} - \rho_{00}) \\ -2\Gamma \cdot \text{Im}[\rho_{01}]^2 \end{bmatrix}. \quad (\text{A13})$$

Under the condition that $\Gamma \ll E$, the oscillations of the phase of the off-diagonal density matrix elements due to E are much faster than the decay dynamics. This condition is thus the regime where the Ehrenfest+R approach can be applied with guaranteed accuracy. Under this condition, one can approximate the coherence as $\rho_{01} \approx |\rho_{01}|e^{iEt}$, thus $\text{Im}[\rho_{01}]^2 \approx |\rho_{01}|^2 \sin^2(Et)$, which can be used to get an approximate expression of Eq. A13.

For the purposes of analysis, it is convenient to average out the insignificant effects that the E -dependent phase oscillations have on the *decay rates* present in Eq. A13. Note that in the actual Ehrenfest+R simulation, \mathcal{L}_{Eh} (Eq. A13) is explicitly used. Thus, following Chen et al.¹⁰, we define a moving average

$$\bar{A} = \frac{1}{\tau} \int_t^{t+\tau} dt' A(t'), \quad (\text{A14})$$

for a timescale τ such that $2\pi/E \ll \tau \ll 1/\Gamma$. The result of performing this moving average will subsequently be called the “time average” of the quantity, although it is important to understand that only the effects that the E -dependent rapid oscillations have on the decay rates have been averaged out while any remaining time dependence is still present in the “time averaged” quantity.

By using $\text{Im}[\rho_{01}]^2 \approx |\rho_{01}|^2 \sin^2(Et)$ and $\overline{\sin^2(Et)} = \frac{1}{2}$, the time average of Eq. A13 is expressed

$$\overline{\mathcal{L}_{\text{Eh}}[\hat{\rho}(t)]} = \begin{bmatrix} \Gamma \cdot |\rho_{01}|^2 \\ iE\rho_{01} - \Gamma \cdot \rho_{01}(\rho_{00} - \rho_{11})/2 \\ -iE\rho_{10} - \Gamma \cdot \rho_{10}(\rho_{00} - \rho_{11})/2 \\ -\Gamma \cdot |\rho_{01}|^2 \end{bmatrix}. \quad (\text{A15})$$

To more clearly understand the dynamics of Eq. A15, it is helpful to determine the *effective* time averaged Liouvillian $\bar{\mathcal{L}}_{\text{Eh}}$ that, when applied to the reduced density matrix, yields the same results as Eq. A15 such that

$$\bar{\mathcal{L}}_{\text{Eh}}[\hat{\rho}(t)] = \overline{\mathcal{L}_{\text{Eh}}[\hat{\rho}(t)]}. \quad (\text{A16})$$

Using the above definition in Eq. A16, one can obtain the effective Liouvillian $\bar{\mathcal{L}}_{\text{Eh}}$ as follows

$$\bar{\mathcal{L}}_{\text{Eh}} = \begin{bmatrix} 0 & 0 & 0 & \bar{k}_{\text{Eh}} \\ 0 & iE - \bar{\gamma}_{\text{Eh}} & 0 & 0 \\ 0 & 0 & -iE - \bar{\gamma}_{\text{Eh}} & 0 \\ 0 & 0 & 0 & -\bar{k}_{\text{Eh}} \end{bmatrix}, \quad (\text{A17})$$

where the time averaged diagonal decay rate \bar{k}_{Eh} and the time averaged off-diagonal decay rate $\bar{\gamma}_{\text{Eh}}$ are expressed as

$$\bar{k}_{\text{Eh}} = \Gamma \cdot |\rho_{01}|^2 / \rho_{11}, \quad (\text{A18})$$

$$\bar{\gamma}_{\text{Eh}} = \Gamma \cdot (\rho_{00} - \rho_{11}) / 2. \quad (\text{A19})$$

The time averaged dynamics in Eq. A15 can thus be expressed as

$$\bar{\mathcal{L}}_{\text{Eh}}[\hat{\rho}(t)] = \begin{bmatrix} \bar{k}_{\text{Eh}}\rho_{11} \\ (iE - \bar{\gamma}_{\text{Eh}})\rho_{01} \\ (-iE - \bar{\gamma}_{\text{Eh}})\rho_{10} \\ -\bar{k}_{\text{Eh}}\rho_{11} \end{bmatrix}. \quad (\text{A20})$$

The dynamics governed by $\bar{\mathcal{L}}_{\text{Eh}}$ (Eq. A17) do not match the Lindblad dynamics governed by \mathcal{L} (Eq. A5) since the decay rates \bar{k}_{Eh} and $\bar{\gamma}_{\text{Eh}}$ from Eqs. A18 and A19 are not constant and depend on the density matrix elements, among other reasons. This is not surprising because it is impossible to recover open system Lindblad dynamics through the deterministic dynamics of a Hamiltonian (Eq. A10). Thus, an additional relaxation propagation (the “+R” stage of the dynamics) is introduced,¹⁰ which is designed to correct both the diagonals and off-diagonals of the reduced density matrix elements in the $\{|0\rangle, |1\rangle\}$ subspace. This *additional* decay process (the +R dynamics) is governed by \mathcal{L}_{R} through

$$\mathcal{L}_{\text{R}}[\hat{\rho}(t)] = \begin{bmatrix} k_{\text{R}}\rho_{11} \\ -\gamma_{\text{R}}\rho_{01} \\ -\gamma_{\text{R}}\rho_{10} \\ -k_{\text{R}}\rho_{11} \end{bmatrix}, \quad (\text{A21})$$

where the diagonal decay rate k_{R} and off-diagonal decay rate γ_{R} are expressed as

$$k_{\text{R}} = 2\Gamma (1 - |\rho_{01}|^2 / \rho_{11}) \text{Im}[e^{i\phi}\rho_{01}/|\rho_{01}|]^2, \quad (\text{A22a})$$

$$\gamma_{\text{R}} = \frac{\Gamma}{2} (1 - \rho_{00} + \rho_{11}). \quad (\text{A22b})$$

The random phase $\phi \in [-\pi, \pi]$ is sampled at the beginning of each trajectory and is kept constant throughout the evolution of that trajectory. The purpose of this phase, in the original context of the Ehrenfest+R development, is to add randomness to the energy of the classical electromagnetic field that couples to the molecules since the Ehrenfest+R method increases the energy of the classical electromagnetic field proportional to k_{R} at each time step due to energy conservation. While this is a necessary feature to accurately describe the classical electromagnetic field, it only affects the quantum dynamics by increasing the variance between the trajectories.

This decay rate k_{R} can be time averaged to yield \bar{k}_{R} as

$$\bar{k}_{\text{R}} = \Gamma (1 - |\rho_{01}|^2 / \rho_{11}). \quad (\text{A23})$$

The effect of the effective time averaged Liouvillian $\bar{\mathcal{L}}_{\text{R}}$ can thus be expressed as

$$\bar{\mathcal{L}}_{\text{R}}[\hat{\rho}(t)] = \begin{bmatrix} \bar{k}_{\text{R}}\rho_{11} \\ -\gamma_{\text{R}}\rho_{01} \\ -\gamma_{\text{R}}\rho_{10} \\ -\bar{k}_{\text{R}}\rho_{11} \end{bmatrix}. \quad (\text{A24})$$

The purpose of constructing the decay rates \bar{k}_R and γ_R as they are in Eqs. A23 and A22b is to satisfy

$$\Gamma = \bar{k}_{\text{Eh}} + \bar{k}_R, \quad (\text{A25a})$$

$$\frac{\Gamma}{2} = \bar{\gamma}_{\text{Eh}} + \gamma_R, \quad (\text{A25b})$$

which consequentially means that the propagation through both stages of dynamics (Ehrenfest and +R) matches Lindblad dynamics such that

$$\mathcal{L}[\hat{\rho}(t)] = \bar{\mathcal{L}}_{\text{Eh}}[\hat{\rho}(t)] + \bar{\mathcal{L}}_R[\hat{\rho}(t)], \quad (\text{A26})$$

where $\mathcal{L}[\hat{\rho}(t)]$, $\bar{\mathcal{L}}_{\text{Eh}}[\hat{\rho}(t)]$, and $\bar{\mathcal{L}}_R[\hat{\rho}(t)]$ are defined in Eq. A6, Eq. A20, and Eq. A24, respectively.

The dynamics associated with the relaxation component $\mathcal{L}_R[\hat{\rho}(t)]$ in Eq. A24 cannot be captured through deterministic dynamics. This is because the off-diagonals must be decohered independent of the diagonals, which requires the use of a random phase that cannot appear in a deterministic method governed solely by a Hamiltonian. Instead of using a modified Hamiltonian in the relaxation stage of the Ehrenfest+R method, the electronic expansion coefficients $\{c_{i,\xi}\}$ of state i and trajectory ξ at each time step are directly modified to attempt to achieve the correct Lindblad dynamics. These coefficient modifications for states $|0\rangle$ and $|1\rangle$ can be summarized as

$$c_1(t+dt) = c_1(t)e^{-k_R dt/2}, \quad (\text{A27a})$$

$$c_0(t+dt) = e^{i\Phi} c_0(t) \sqrt{\frac{|c_0(t)|^2 + |c_1(t)|^2 (1 - e^{-k_R dt})}{|c_0(t)|^2}}, \quad (\text{A27b})$$

with k_R expressed in Eq. A22a. Here, the coefficients $c_1(t+dt)$ and $c_0(t+dt)$ are for a particular trajectory ξ (same as we defined in Eq. 30), and to make our following notation concise, we drop the label ξ in these coefficients. Further, $e^{i\Phi}$ is a random phase factor that enforces dephasing with the rate of γ_R (Eq. A22b). The random phase $\Phi \in [-\pi, \pi]$ is governed by the following distribution

$$\mathcal{P}(\Phi) = \begin{cases} \frac{1}{2\pi}, & RN < \gamma_R dt \\ \delta(\Phi), & RN \geq \gamma_R dt \end{cases} \quad (\text{A28})$$

where $\mathcal{P}(\Phi)$ is the probability distribution of the random phase Φ , $\delta(\Phi)$ is the Dirac delta distribution, and RN is a random number in the range of $RN \in [0, 1]$. The “+R” relaxation stage of the Ehrenfest+R approach is summarized in Eq. A27a, Eq. A27b, and Eq. A28. This provides an effective Poisson process for incorporating decoherence. Generalizing this approach to multiple state has been proposed and tested as well¹¹, where the coefficients $\{c_{j,\xi}\}$ for $|j\rangle \notin \{|0\rangle, |1\rangle\}$ are not changed by the Lindbladian time evolution, such that

$$c_{j,\xi}(t+dt) = c_{j,\xi}(t). \quad (\text{A29})$$

What has not yet been determined from this analysis, however, is whether the proposed relaxation method in

Eq. A27a, Eq. A27b, and Eq. A28 corresponds to the effective time averaged Liouvillian in Eq. A24 or not. As will be shown in the next section, the proposed relaxation stage does not correspond to this Liouvillian, and the γ_R decay rate must be modified in order to satisfy Eq. A26.

Appendix B: Fixing the Ehrenfest+R Approach

To understand how these coefficient modifications in Eq. A27a and Eq. A27b affect the overall dynamics, it is best to work backwards to determine the effective Liouvillian $\bar{\mathcal{L}}_R$ that generated these relaxation dynamics, and figure out whether Eq. A26 is satisfied. The modified coefficients can be written in the density matrix form using the outer product as

$$\begin{aligned} & \begin{bmatrix} c_0(t+dt) \\ c_1(t+dt) \end{bmatrix} [c_0^*(t+dt), c_1^*(t+dt)] \\ &= \begin{bmatrix} |c_0(t+dt)|^2 \\ c_0(t+dt)c_1^*(t+dt) \\ c_1(t+dt)c_0^*(t+dt) \\ |c_1(t+dt)|^2 \end{bmatrix}. \end{aligned} \quad (\text{B1})$$

Due to the presence of a random phase, the expectation value of Eq. B1 is what the trajectory-averaged density matrix will converge towards and will be treated as the result of operating the effective Liouvillian \mathcal{L}_R onto the density matrix, which can be written as

$$\begin{aligned} e^{\mathcal{L}_R dt} [\hat{\rho}(t)] &= \begin{bmatrix} \langle |c_0(t+dt)|^2 \rangle \\ \langle c_0(t+dt)c_1^*(t+dt) \rangle \\ \langle c_1(t+dt)c_0^*(t+dt) \rangle \\ \langle |c_1(t+dt)|^2 \rangle \end{bmatrix} \\ &= \begin{bmatrix} |c_0(t)|^2 + |c_1(t)|^2 (1 - e^{-k_R dt}) \\ c_0(t)c_1^*(t) \langle e^{i\Phi} \rangle e^{-k_R dt/2} \sqrt{\frac{|c_0(t)|^2 + |c_1(t)|^2 (1 - e^{-k_R dt})}{|c_0(t)|^2}} \\ c_1(t)c_0^*(t) \langle e^{-i\Phi} \rangle e^{-k_R dt/2} \sqrt{\frac{|c_0(t)|^2 + |c_1(t)|^2 (1 - e^{-k_R dt})}{|c_0(t)|^2}} \\ |c_1(t)|^2 e^{-k_R dt} \end{bmatrix} \end{aligned} \quad (\text{B2})$$

where we have explicitly used the expressions in Eq. A27a- A27b to write down these coefficients. The superoperator $e^{\mathcal{L}_R dt}$ can be determined from Eq. B2 by identifying the coefficients $|c_0(t)|^2$, $c_0(t)c_1^*(t)$, $c_1(t)c_0^*(t)$, and $|c_1(t)|^2$ on the left-hand side as the density matrix elements ρ_{00} , ρ_{01} , ρ_{10} , and ρ_{11} , respectively, and considering the terms that these density matrix elements multiply with as the rates that come from $e^{\mathcal{L}_R dt}$. This superoperator can thus be identified as

$$e^{\mathcal{L}_R dt} = \begin{bmatrix} 1 & 0 & 0 & 1 - e^{-k_R dt} \\ 0 & \beta & 0 & 0 \\ 0 & 0 & \beta^* & 0 \\ 0 & 0 & 0 & e^{-k_R dt} \end{bmatrix}, \quad (\text{B3})$$

with $\beta = \langle e^{i\Phi} \rangle e^{-k_R dt/2} \sqrt{\frac{|c_0(t)|^2 + |c_1(t)|^2 (1 - e^{-k_R dt})}{|c_0(t)|^2}}$. Taking the matrix logarithm of $e^{\mathcal{L}_R dt}$ yields the Liouvillian

\mathcal{L}_R as

$$\mathcal{L}_R = \begin{bmatrix} 0 & 0 & 0 & k_R \\ 0 & \frac{\ln \beta}{dt} & 0 & 0 \\ 0 & 0 & \frac{\ln \beta^*}{dt} & 0 \\ 0 & 0 & 0 & -k_R \end{bmatrix}. \quad (\text{B4})$$

The k_R rate in the right hand column of Eq. B4 can be approximated by the time averaged \bar{k}_R to express the effective time averaged Liouvillian $\bar{\mathcal{L}}_R$ as

$$\bar{\mathcal{L}}_R = \begin{bmatrix} 0 & 0 & 0 & \bar{k}_R \\ 0 & \frac{\ln \beta}{dt} & 0 & 0 \\ 0 & 0 & \frac{\ln \beta^*}{dt} & 0 \\ 0 & 0 & 0 & -\bar{k}_R \end{bmatrix}. \quad (\text{B5})$$

Eq. B5 is the effective Liouvillian that describes the dynamics due to the coefficient modifications in Eqs. A27a and A27b. The total Ehrenfest+R dynamics can thus be described by the sum of the Liouvillians $\bar{\mathcal{L}}_{\text{Eh}}$ and $\bar{\mathcal{L}}_R$, which is

$$\bar{\mathcal{L}}_{\text{Eh}} + \bar{\mathcal{L}}_R = \begin{bmatrix} 0 & 0 & 0 & \bar{k}_{\text{Eh}} + \bar{k}_R \\ 0 & iE - \bar{\gamma}_{\text{Eh}} + \frac{\ln \beta}{dt} & 0 & 0 \\ 0 & 0 & -iE - \bar{\gamma}_{\text{Eh}} + \frac{\ln \beta^*}{dt} & 0 \\ 0 & 0 & 0 & -\bar{k}_{\text{Eh}} - \bar{k}_R \end{bmatrix}. \quad (\text{B6})$$

If the Ehrenfest+R method has been successful, this sum in Eq. B6 should be equivalent to the Lindblad Liouvillian in Eq. A5. The $\bar{k}_{\text{Eh}} + \bar{k}_R$ and $-\bar{k}_{\text{Eh}} - \bar{k}_R$ elements in the right-hand column of Eq. B6 match the elements inside the Lindblad Liouvillian \mathcal{L} (Eq. A5), Γ and $-\Gamma$, respectively, due to Eq. A22a. The elements in the middle two columns of Eq. B6 require closer inspection. The expectation value inside of α can be evaluated as

$$\langle e^{\pm i\Phi} \rangle = 1 - \gamma_R dt \approx e^{-\gamma_R dt}, \quad (\text{B7})$$

such that the expectation value will be treated as an approximation of the exponential function in order to extract γ_R outside of the logarithm. This approximation is present due to the choice of a Poisson rate process in determining the distribution of the random phase in Eq. A28 which results in the decoherence being a first order approximation of an exponential decay. Thus, the chosen distribution for the random phase Φ requires $\gamma_R dt \ll 1$ for accuracy. Treating the expectation value as the exponential decay in Eq. B7, the leftmost non-zero

element of Eq. B6 can be evaluated as

$$\begin{aligned} iE - \bar{\gamma}_{\text{Eh}} + \frac{\ln \beta}{dt} &\approx iE - \bar{\gamma}_{\text{Eh}} - \gamma_R \\ &+ \frac{1}{dt} \ln \left(e^{-k_R dt/2} \sqrt{\frac{|c_0(t)|^2 + |c_1(t)|^2 (1 - e^{-k_R dt})}{|c_0(t)|^2}} \right) \\ &= iE - \frac{\Gamma}{2} \\ &+ \frac{1}{dt} \ln \left(e^{-k_R dt/2} \sqrt{\frac{|c_0(t)|^2 + |c_1(t)|^2 (1 - e^{-k_R dt})}{|c_0(t)|^2}} \right), \end{aligned} \quad (\text{B8})$$

where Eq. A22b has been used to substitute $\Gamma/2$ in for $\bar{\gamma}_{\text{Eh}} + \gamma_R$. Comparing the effective Liouvillian in Eq. B6 and the actual Lindblad Liouvillian in Eq. A5, the terms $\bar{k}_{\text{Eh}} + \bar{k}_R = \Gamma$ match. However, the term $iE - \bar{\gamma}_{\text{Eh}} + \frac{\ln \beta}{dt}$ in Eq. B6 fails to match the term $iE - \frac{\Gamma}{2}$ in Eq. A5, by the difference of the extra last term in Eq. B8. The presence of this extraneous term is due to the modification of the magnitudes of the coefficients in Eqs. A27a and A27b. The expression inside of the logarithm in Eq. B8 is the ratio of the modified coefficient magnitudes to the original coefficient magnitudes. These magnitude modifications change the coherence between the ground and excited states (as well as all other states in larger dimensional systems) thus their impact must be taken into consideration in the off-diagonal decay procedure in order to match Lindblad dynamics.

To redeem the Ehrenfest+R approach, one can modify the decay rate γ'_R to absorb this additional term (the last term in Eq. B8), such that the following equality is explicitly enforced

$$iE - \bar{\gamma}_{\text{Eh}} + \frac{\ln \beta}{dt} \approx iE - \frac{\Gamma}{2}, \quad (\text{B9})$$

in addition to $\Gamma = \bar{k}_{\text{Eh}} + \bar{k}_R$, thus actually enforcing $\bar{\mathcal{L}}_{\text{Eh}} + \bar{\mathcal{L}}_R = \mathcal{L}$. The modified decay rate γ'_R is thus defined as

$$\begin{aligned} \gamma'_R &= \gamma_R \\ &+ \frac{1}{dt} \ln \left(e^{-k_R dt/2} \sqrt{\frac{|c_0(t)|^2 + |c_1(t)|^2 (1 - e^{-k_R dt})}{|c_0(t)|^2}} \right), \end{aligned} \quad (\text{B10})$$

which can be more conveniently expressed purely in terms of coefficients as

$$\begin{aligned} \gamma'_R &= \frac{\Gamma}{2} (1 - |c_0(t)|^2 + |c_1(t)|^2) \\ &+ \frac{1}{dt} \ln \left(\frac{|c_0(t+dt)c_1^*(t+dt)|}{|c_0(t)c_1^*(t)|} \right), \end{aligned} \quad (\text{B11})$$

where the expression inside the logarithm in Eq. B10 has been replaced by the ratio of the magnitudes of the modified coefficients to the original coefficients (when explicitly using Eq. A27a and Eq. A27b). Eq. B11 is the correct

modification regardless of whether a linear approximation of the exponential function is used when modifying the magnitudes of the coefficients (as has been done in most applications of the Ehrenfest+R method). This is validated numerically in Fig. 5 where panels a and c are the results of the Ehrenfest+R method with the original γ_R (and a linearization of the exponential when calculating the modified coefficient magnitudes) while panels b and d are the results when replacing γ_R with γ'_R from Eq. B11.

As opposed to the Ehrenfest+R method, the \mathcal{L} -MFE method generates the identical Liouvillian $\mathcal{L}_{\hat{L}}$ (Eq. A2) associated with the quantum jump operator \hat{L} . This can be verified by using the procedure outlined in Eq. B1-Eq. B2

$$e^{\mathcal{L}_{\hat{L}}dt} [\hat{\rho}(t)] = \begin{bmatrix} \langle |c_0(t+dt)|^2 \rangle \\ \langle c_0(t+dt)c_1^*(t+dt) \rangle \\ \langle c_1(t+dt)c_0^*(t+dt) \rangle \\ \langle |c_1(t+dt)|^2 \rangle \end{bmatrix} \quad (\text{B12})$$

$$= \begin{bmatrix} |c_0(t)|^2 + (1 - e^{-\Gamma dt}) |c_1(t)|^2 \\ c_0(t)c_1^*(t) \langle e^{i\theta} \rangle e^{-\Gamma dt/2} \sqrt{\frac{|c_0(t)|^2 + |c_1(t)|^2(1 - e^{-\Gamma dt})}{|c_0(t)|^2}} \\ c_1(t)c_0^*(t) \langle e^{-i\theta} \rangle e^{-\Gamma dt/2} \sqrt{\frac{|c_0(t)|^2 + |c_1(t)|^2(1 - e^{-\Gamma dt})}{|c_0(t)|^2}} \\ |c_1(t)|^2 e^{-\Gamma dt} \end{bmatrix}.$$

Using the explicit expression of $\langle e^{\pm i\theta} \rangle$ (see Eq. 59) inside Eq. B12, we can express the effective Liouvillian as

$$e^{\mathcal{L}_{\hat{L}}dt} = \begin{bmatrix} 1 & 0 & 0 & 1 - e^{-\Gamma dt} \\ 0 & e^{-\Gamma dt/2} & 0 & 0 \\ 0 & 0 & e^{-\Gamma dt/2} & 0 \\ 0 & 0 & 0 & e^{-\Gamma dt} \end{bmatrix}. \quad (\text{B13})$$

Taking the matrix logarithm of the above $e^{\mathcal{L}_{\hat{L}}dt}$ indeed yields the Lindblad jump Liouvillian $\mathcal{L}_{\hat{L}}$ in Eq. A2. One can also generalize the above argument for the many states situation as described in Eq. 24.

Appendix C: Molecular Hamiltonian of the Isomerization Model System

In this section, we provide detailed expressions for the model matter Hamiltonian used in this study. The molecular Hamiltonian \hat{H}_M is described by a model system that undergoes an isomerization reaction^{58,65}

$$\hat{H}_M = \hat{T}_R + E_g(R)|g\rangle\langle g| + E_e(R)|e\rangle\langle e|. \quad (\text{C1})$$

Here, $|\alpha\rangle \in \{|g\rangle, |e\rangle\}$ represents the electronic ground or excited states, R represents the nuclear reaction coordinate, and \hat{T}_R is the nuclear kinetic energy operator. The electronic potentials $E_g(R)$ and $E_e(R)$ are modeled with the following expressions

$$E_g(R) = \frac{v_1(R) + v_2(R)}{2} - \sqrt{D_1^2 + \frac{(v_1(R) - v_2(R))^2}{4}},$$

$$E_e(R) = \frac{v_3(R) + v_4(R)}{2} - \sqrt{D_2^2 + \frac{(v_3(R) - v_4(R))^2}{4}},$$

where $v_i(R) = A_i + B_i(R - R_i)^2$, and the rest of the parameters (in a.u.) are tabulated below

i	A_i	B_i	R_i	D_i
1	0.049244	0.183747	-0.75	0.073499
2	0.010657	0.183747	0.85	0.514490
3	0.428129	0.183747	-1.15	-
4	0.373005	0.146997	1.25	-

Note that the derivative coupling $\langle g|\nabla_R|e\rangle$ is not included in the model system. With this assumption, both the $|g\rangle$ and $|e\rangle$ states effectively become diabatic states. Numerical simulations that do consider these derivative couplings can be found in the Supporting Information of Ref. 58.

Appendix D: Molecular Cavity QED with Cavity Losses

The lifetime of the cavity mode is finite, due to the coupling between the cavity mode and the far-field photon modes outside the cavity described by the environmental Hamiltonian

$$\hat{H}_E = \sum_k \hbar\omega_k (\hat{b}_k^\dagger \hat{b}_k + \frac{1}{2}), \quad (\text{D1})$$

where \hat{b}_k^\dagger and \hat{b}_k are the raising and lowering operators, respectively, for far-field mode k . The interactions between the cavity mode and the far-field modes can be described by the following Gardiner-Collett interaction Hamiltonian⁶⁶⁻⁶⁸ (denote as the system-environment interactions in Eq. 1) as

$$\hat{H}_I = (\hat{a}^\dagger + \hat{a}) \otimes \sum_k \hbar g_k (\hat{b}_k^\dagger + \hat{b}_k), \quad (\text{D2})$$

where the coupling strength between the cavity mode and the k th environmental mode is g_k , characterized by a spectral density,^{13,69} and we have ignored $\hat{\mathcal{L}}_e$ and $\hat{\mathcal{L}}_R$ in \hat{H}_I . This Hamiltonian can be rigorously derived from QED first principles, and has been used to investigate polariton quantum dynamics in a dissipative cavity.^{13,69}

Using the molecule-cavity hybrid Hamiltonian \hat{H}_{QED} in Eq. 77 as \hat{H}_S and the jump operator¹⁴ \hat{L}_S in Eq. 81 to describe cavity losses, one can rewrite Eq. 12 (without explicitly showing $\hat{\mathcal{L}}_e$ and $\hat{\mathcal{L}}_R$) as follows

$$\frac{d\hat{\rho}_S}{dt} = -\frac{i}{\hbar} [\hat{H}_S, \hat{\rho}_S] + \Gamma \left(\hat{a} \hat{\rho}_S \hat{a}^\dagger - \frac{1}{2} \{ \hat{a}^\dagger \hat{a}, \hat{\rho}_S \} \right), \quad (\text{D3})$$

where the term $-\frac{1}{2} \{ \hat{a}^\dagger \hat{a}, \hat{\rho}_S \}$ causes population decay as well as decoherence among states, whereas the $\hat{a} \hat{\rho}_S \hat{a}^\dagger$ term (refilling term) makes the population reappear in the new state that the decay leads to. An equivalent way to write the Lindblad master equation is

$$\frac{d\hat{\rho}_S}{dt} = -\frac{i}{\hbar} \left(\hat{H}_{\text{eff}} \hat{\rho}_S - \hat{\rho}_S \hat{H}_{\text{eff}}^\dagger \right) + \Gamma \hat{a} \hat{\rho}_S \hat{a}^\dagger, \quad (\text{D4})$$

where the effective Hamiltonian is

$$\hat{H}_{\text{eff}} = \hat{H}_S - i \frac{\hbar\Gamma}{2} \hat{a}^\dagger \hat{a}. \quad (\text{D5})$$

The same expression has been used in the development of the stochastic Schrödinger equation^{35–37} (see Eq. 73) that is equivalent to Lindblad dynamics. Thus, when completely ignoring the refilling term $\Gamma \hat{a} \hat{\rho}_S \hat{a}^\dagger$, one can approximate Lindblad dynamics as the time dependent Schrödinger equation (TDSE) with the complex Hamiltonian \hat{H}_{eff} , which has been used in several recent works on molecular cavity QED.^{15,21–25} In the situations where the refilling term is negligible, the dynamics can equivalently be described by using the Schrödinger equation of a wave function evolving with the effective Hamiltonian. However, for the applications considered in the current work in Fig. 7, one cannot ignore the $\Gamma \hat{a} \hat{\rho}_S \hat{a}^\dagger$ term as we do care about the population refilling in the $|g, 0\rangle$ state, as well as the proper decoherence among these states.

Note that despite the common usage of the Lindblad jump operator $\hat{L}_S = \hat{a} \otimes \hat{I}_e \otimes \hat{I}_R$ (Eq. 81) for describing cavity losses,¹⁴ this jump operator is actually derived by considering the simpler system Hamiltonian $\hat{H}_S = \hbar\omega_c (\hat{a}^\dagger \hat{a} + \frac{1}{2}) \otimes \hat{I}_e \otimes \hat{I}_R$ without explicit consideration for the matter Hamiltonian or molecule-cavity interactions in \hat{H}_{QED} . Thus, Eq. D3 should be viewed as a phenomenological equation, and the correct Lindblad master equation for cavity QED should be derived starting from the total Hamiltonian^{70,71} $\hat{H}_T = \hat{H}_{\text{QED}} + \hat{H}_E + \hat{H}_I$, where \hat{H}_E and \hat{H}_I are expressed in Eq. D1 and Eq. D2, respectively. The details of the microscopic derivation of the Lindblad master equation for the Jaynes-Cummings model with cavity losses, as well as for comparison with Eq. D3, can be found in Ref. 70.

- ¹L. Wang, A. Akimov, and O. V. Prezhdo, *The Journal of Physical Chemistry Letters* **7**, 2100 (2016).
- ²B. F. E. Curchod and T. J. Martínez, *Chem. Rev.* **118**, 3305 (2018).
- ³J. C. Tully, *J. Chem. Phys.* **93**, 1061 (1990).
- ⁴Y.-S. Wang, P. Nijjar, X. Zhou, D. I. Bondar, and O. V. Prezhdo, *The Journal of Physical Chemistry B* **124**, 4326 (2020).
- ⁵Z. Jin and J. E. Subotnik, *Journal of Chemical Theory and Computation* **17**, 614 (2021).
- ⁶A. Kirrander and M. Vacher, “Ehrenfest methods for electron and nuclear dynamics,” in *Quantum Chemistry and Dynamics of Excited States* (John Wiley & Sons, Ltd, 2020) Chap. 15, pp. 469–497.
- ⁷M. Thoss and G. Stock, *Phys. Rev. A* **59**, 64 (1999).
- ⁸J. R. Mannouch and J. O. Richardson, *J. Chem. Phys.* **153**, 194109 (2020).
- ⁹S. J. Cotton and W. H. Miller, *J. Chem. Phys.* **150**, 194110 (2019).
- ¹⁰H.-T. Chen, T. E. Li, M. Sukharev, A. Nitzan, and J. E. Subotnik, *J. Chem. Phys.* **150**, 044102 (2019).
- ¹¹H.-T. Chen, T. E. Li, M. Sukharev, A. Nitzan, and J. E. Subotnik, *J. Chem. Phys.* **150**, 044103 (2019).
- ¹²H.-T. Chen, T. E. Li, A. Nitzan, and J. E. Subotnik, *Phys. Rev. A* **100**, 010101 (2019).
- ¹³J. Pino, F. Schroder, A. Chin, J. Feist, and F. Garcia-Vidal, *Phys. Rev. B* **98**, 165416 (2018).
- ¹⁴J. Torres-Sánchez and J. Feist, *J. Chem. Phys.* **154**, 014303 (2021).

- ¹⁵S. Felicetti, J. Fregoni, T. Schnappinger, S. Reiter, R. de Vivie-Riedle, and J. Feist, *The Journal of Physical Chemistry Letters* **11**, 8810 (2020).
- ¹⁶E. Davidsson and M. Kowalewski, *J. Chem. Phys.* **153**, 234304 (2020).
- ¹⁷D. Wellnitz, G. Pupillo, and J. Schachenmayer, *J. Chem. Phys.* **154**, 054104 (2021).
- ¹⁸T. C. Berkelbach, D. R. Reichman, and T. E. Markland, *The Journal of Chemical Physics* **136**, 034113 (2012).
- ¹⁹T. C. Berkelbach, T. E. Markland, and D. R. Reichman, *The Journal of Chemical Physics* **136**, 084104 (2012).
- ²⁰A. J. Schile and D. T. Limmer, *J. Chem. Phys.* **151**, 014106 (2019).
- ²¹P. Antoniou, F. Suchanek, J. F. Varner, and J. J. Foley, *The Journal of Physical Chemistry Letters* **11**, 9063 (2020).
- ²²C. L. Cortes, M. Otten, and S. K. Gray, *J. Chem. Phys.* **152**, 084105 (2020).
- ²³I. Wilson-Rae and A. Imamoglu, *Phys. Rev. B* **65**, 235311 (2002).
- ²⁴F. Kossoski and M. Barbatti, *Chem. Sci.* **11**, 9827 (2020).
- ²⁵I. S. Ulusoy and O. Vendrell, *J. Chem. Phys.* **153**, 044108 (2020).
- ²⁶K. Müller, K. A. Fischer, A. Rundquist, C. Dory, K. G. Lagoudakis, T. Sarmiento, Y. A. Kelaita, V. Borish, and J. Vučković, *Phys. Rev. X* **5**, 031006 (2015).
- ²⁷G. Groenhof, C. Climent, J. Feist, D. Morozov, and J. J. Toppari, *The Journal of Physical Chemistry Letters* **10**, 5476 (2019).
- ²⁸R. H. Tichauer, J. Feist, and G. Groenhof, *J. Chem. Phys.* **154**, 104112 (2021).
- ²⁹M. Du, J. A. Campos-Gonzalez-Angulo, and J. Yuen-Zhou, *The Journal of Chemical Physics* **154**, 084108 (2021).
- ³⁰J. Fregoni, G. Granucci, E. Coccia, M. Persico, and S. Corni, *Nature Communications* **9**, 4688 (2018).
- ³¹G. Lindblad, *Commun. Math. Phys.* **48**, 119 (1976).
- ³²D. Manzano, *AIP Advances* **10**, 025106 (2020).
- ³³H.-P. Breure and F. Petruccione, “The theory of open quantum systems,” (Oxford, 2006).
- ³⁴M. Moodley and F. Petruccione, *Phys. Rev. A* **79**, 042103 (2009).
- ³⁵K. Mølmer, Y. Castin, and J. Dalibard, *J. Opt. Soc. Am. B* **10**, 524 (1993).
- ³⁶J. Dalibard and Y. Castin, *Phys. Rev. Lett.* **68**, 580 (1992).
- ³⁷G. C. Ghirardi, P. Pearle, and A. Rimini, *Phys. Rev. A* **42**, 78 (1999).
- ³⁸O. V. Prezhdo, *J. Chem. Phys.* **111**, 8366 (1999).
- ³⁹T. E. Li, H.-T. Chen, and J. E. Subotnik, *Journal of Chemical Theory and Computation* **15**, 1957 (2019).
- ⁴⁰H.-T. Chen, T. E. Li, A. Nitzan, and J. E. Subotnik, *The Journal of Physical Chemistry Letters* **10**, 1331 (2019).
- ⁴¹S. J. Cotton and W. H. Miller, *J. Chem. Phys.* **139**, 234112 (2013).
- ⁴²S. J. Cotton and W. H. Miller, *J. Phys. Chem. A* **117**, 7190 (2013).
- ⁴³S. J. Cotton and W. H. Miller, *J. Chem. Phys.* **150**, 194110 (2019).
- ⁴⁴B. M. Weight, A. Mandal, and P. Huo, *J. Chem. Phys.* **155**, 084106 (2021).
- ⁴⁵P. Huo and D. F. Coker, *J. Chem. Phys.* **135**, 201101 (2011).
- ⁴⁶J. R. Mannouch and J. O. Richardson, *J. Chem. Phys.* **153**, 194110 (2020).
- ⁴⁷I. de Vega and D. Alonso, *Rev. Mod. Phys.* **89**, 015001 (2017).
- ⁴⁸D. A. Lidar, “Lecture notes on the theory of open quantum systems,” (2020), arXiv:1902.00967 [quant-ph].
- ⁴⁹K. Hornberger, “Introduction to decoherence theory,” in *Entanglement and Decoherence: Foundations and Modern Trends*, edited by A. Buchleitner, C. Viviescas, and M. Tiersch (Springer Berlin Heidelberg, Berlin, Heidelberg, 2009) pp. 221–276.
- ⁵⁰K. Temme, F. Pastawski, and M. J. Kastoryano, *J. Phys. A: Math. Theor.* **47**, 405303 (2014).
- ⁵¹V. V. Albert and L. Jiang, *Phys. Rev. A* **89**, 022118 (2014).
- ⁵²J. C. Tully, *J. Chem. Phys.* **137**, 22A301 (2012).
- ⁵³M. Vacher, D. Mende-Tapia, M. J. Bearpark, and M. A. Robb, *Theoretical Chemistry Accounts* **133**, 1505 (2014).

- ⁵⁴R. da Silva Oliboni, G. Bortolini, A. Torres, and L. G. C. Rego, *The Journal of Physical Chemistry C* **120**, 27688 (2016).
- ⁵⁵X. Li, J. C. Tully, H. B. Schlegel, and M. J. Frisch, *J. Chem. Phys.* **123**, 084106 (2005).
- ⁵⁶A. J. Schile and D. T. Limmer, *J. Chem. Phys.* **149**, 214109 (2018).
- ⁵⁷A. Arnold, F. Fagnola, and L. Neumann, in *Quantum Probability and Related Topics* (2007) pp. 23–48.
- ⁵⁸A. Mandal and P. Huo, *J. Phys. Chem. Lett.* **10**, 5519 (2019).
- ⁵⁹M. A. D. Taylor, A. Mandal, W. Zhou, and P. Huo, *Phys. Rev. Lett.* **125**, 123602 (2020).
- ⁶⁰J. Johansson, P. Nation, and F. Nori, *Computer Physics Communications* **183**, 1760 (2012).
- ⁶¹J. Johansson, P. Nation, and F. Nori, *Computer Physics Communications* **184**, 1234 (2013).
- ⁶²M. Kowalewski, K. Bennett, and S. Mukamel, *J. Chem. Phys.* **144**, 054309 (2016).
- ⁶³L. Qiu, A. Mandal, O. Morshed, M. T. Meidenbauer, W. Girten, P. Huo, A. N. Vamivakas, and T. D. Krauss, *J. Phys. Chem. Lett.* **12**, 5030 (2021).
- ⁶⁴A. V. Akimov, R. Long, and O. V. Prezhdo, *J. Chem. Phys.* **140**, 194107 (2014).
- ⁶⁵J. Galego, F. J. Garcia-Vidal, and J. Feist, *Phys. Rev. Lett.* **119**, 136001 (2017).
- ⁶⁶S. Dutra and G. Nienhuis, *J. Opt. B: Quantum Semiclass.* **2**, 584 (2000).
- ⁶⁷S. Dutra and G. Nienhuis, *Phys. Rev. A* **62**, 063805 (2000).
- ⁶⁸S. Dutra and G. Nienhuis, *Cavity Quantum Electrodynamics: The Strange Theory of Light in a Box* (2004).
- ⁶⁹A. Nourmandipour and M. K. Tavassoly, *J. Phys. B: At. Mol. Opt. Phys.* **48**, 165502 (2015).
- ⁷⁰M. Scala, B. Militello, A. Messina, J. Piilo, and S. Maniscalco, *Phys. Rev. A* **75**, 013811 (2007).
- ⁷¹S. Ozaki and H. Nakazato, *Phys. Rev. A* **103**, 053713 (2021).